Eur. Phys. J. C (2024) 84:667
https://doi.org/10.1140/epjc/s10052-024-12992-3

THE EUROPEAN PHYSICAL JOURNAL C

Regular Article - Theoretical Physics

Revisiting cosmological constraints on supersymmetric SuperWIMPs

Meera Deshpande[1], **Jan Hamann**[2], **Dipan Sengupta**[1,2,a], **Martin White**[1], **Anthony G. Williams**[1], **Yvonne Y. Y. Wong**[2]

[1] Department of Physics, ARC Centre of Excellence for Dark Matter Particle Physics, The University of Adelaide, Adelaide, SA 5005, Australia
[2] School of Physics, Sydney Consortium for Particle Physics and Cosmology, The University of New South Wales, Sydney, NSW 2052, Australia

Received: 19 September 2023 / Accepted: 3 June 2024 / Published online: 5 July 2024

Abstract SuperWIMPs are extremely weakly interacting massive particles that inherit their relic abundance from late decays of frozen-out parent particles. Within supersymmetric models, gravitinos and axinos represent two of the most well motivated superWIMPs. In this paper we revisit constraints on these scenarios from a variety of cosmological observations that probe their production mechanisms as well as the superWIMP kinematic properties in the early Universe. We consider in particular observables of Big Bang Nucleosynthesis and the Cosmic Microwave Background (spectral distortion and anisotropies), which limit the fractional energy injection from the late decays, as well as warm and mixed dark matter constraints derived from the Lyman-α forest and other small-scale structure observables. We discuss complementary constraints from collider experiments, and argue that cosmological considerations rule out a significant part of the gravitino and the axino superWIMP parameter space.

1 Introduction

The pursuit of signatures of beyond-the-Standard-Model (BSM) physics and an explanation for the dark matter of the Universe has been the holy grail for particle physicists for over three decades. To this end, the Large Hadron Collider (LHC) has probed large swathes of parameter space in a variety of well motivated BSM models. These include Supersymmetry (SUSY), the leading BSM theory that not only solves the hierarchy problem but also provides a slew of particle candidates for the dark matter. Within the context of specific SUSY breaking scenarios as well as simplified models, null measurements at the LHC have translated into constraints on a significant chunk of SUSY particles in the GeV-to-TeV mass range [1–3].

However, SUSY/BSM searches at the LHC rely primarily on prompt decays or, at best, decays with proper lengths of $\mathcal{O}(10-100)$ m in the so-called long-lived particle (LLP) searches [4,5]. These searches are further subject to the constraints that the produced particles are within kinematic reach of the LHC, i.e., their masses are at most a few TeV, and that they are produced with a cross-section sufficient to generate a detectable signal over the enormous Standard-Model background. Extremely weakly-interacting particles and/or those with very long lifetimes – many of which also reside in well-motivated SUSY/BSM model and parameter spaces – are thus inherently out of the LHC's reach, even if their masses lie within the conventional GeV-to-TeV collider window.

Interestingly, when the proper decay lengths/lifetimes of these particles exceed $\mathcal{O}(10)$ m, a second, albeit less conventional, window to explore their properties opens up. Disregarding concerns of naturalness, scenarios of extremely long particle lifetimes could be easily realised in a wide range of BSM theories by particle masses and couplings spanning orders of magnitude (e.g., $m \sim \mathcal{O}(1)$ MeV $-\,\mathcal{O}(100)$ TeV). In the context of SUSY, these scenarios fall under the superWIMP class of models [6,7], wherein quasi-stable particles can be efficiently produced in the early Universe and decay at a very late time, i.e., $t \gg \mathcal{O}(1)$ s post-Big Bang, during the standard cosmological history. Regardless of whether these quasi-stable particles can account for all of the observed dark matter abundance of the Universe at early times, late-decaying particles leave potentially observable signatures in the cosmic microwave background radiation (CMB), as well as the light element abundances from Big Bang Nucleosynthesis (BBN) and the large-scale matter distribution, particularly the Lyman-α (Lyα) forest. Measurements of these observables can in turn be used to probe and constrain

[a] e-mail: dipan.sengupta@adelaide.edu.au (corresponding author)

regions of SUSY/BSM parameter space inaccessible to collider searches.

As a concrete example, consider the following: in R-parity-conserving SUSY, the conventional lightest SUSY particle (LSP) dark matter candidate is the lightest neutralino, superpartner of the electroweak gauge particles. With masses $m_{\rm LSP} \sim \mathcal{O}(0.1\text{–}1)$ TeV and weak-like interactions with the Standard Model (SM), the neutralino easily satisfies the observed relic abundance of the Universe and has a range of signatures at collider physics experiments, as well as at direct and indirect dark matter searches [8,9]. However, in models of Supergravity or in SUSY models extended to include the axion, the lightest neutralino may not be the LSP but can decay to lighter particles of these theories, such as the gravitino $\tilde{G}$ or the axino $\tilde{a}$. That is, the neutralino is now the next-to-lightest supersymmetric particle (NLSP), while the gravitino or the axino serves as the LSP [6,7,10–12].

In the latter scenarios, the decay widths of the NLSP neutralino to $\tilde{G}$ and $\tilde{a}$ are generally suppressed, either by the Planck mass $m_{\rm Pl}$ or by the axion decay constant f_a, such that the lifetime of the NLSP can be much longer than its freeze-out time scale. In this case, the decay of the NLSP can also generate an axino or gravitino population. Provided that the reheating temperature is low enough to avoid significant production of $\tilde{G}$ or $\tilde{a}$ from thermal scattering in the very early Universe [13], it is the late-time NLSP-to-LSP decay process that dominates the final $\tilde{G}$ or $\tilde{a}$ abundance.

Then, the relic LSP production can be thought of as a two-stage process. First, a neutralino NLSP population is produced by interactions with the SM.[1] Such a neutralino population with the right observed relic density can build up either via the usual thermal freeze-out mechanism through annihilations with SM particles, or via freeze-in if extremely-weakly coupled to the parent SUSY and other SM particles. Irrespective of the details of this first step, at very late times the neutralino NLSP decays into the gravitino or axino LSP, constituting the second step of the LSP production process. The gravitino or axino LSP thus generated – dubbed as SUSY superWIMPs in the literature – can provide part or all of the observed dark matter in the Universe [6,16–18].

Because superWIMPs are extremely weakly coupled – the interactions of the gravitino and axino are $m_{\rm Pl}$- or f_a-suppressed – prompt searches at colliders are insensitive to a large part of their parameter space. Only a small sliver can potentially be probed [11,12,18–26,26–29], via searches for long-lived particles by ATLAS, CMS, or future experiments such as FASER [30] and Mathusla [31].[2] In a similar vein, bounds on the superWIMP parameter space from direct and indirect dark matter searches are practically non-existent. Our best prospects for probing and constraining superWIMP scenarios lie in cosmological observations.

A number of early studies have considered how gravitino superWIMPs can be probed cosmologically [6,7,22,34–36], based primarily on the premise that electromagnetic and/or hadronic energy released from the NLSP-to-LSP decay has consequences for the light element yields from BBN and the CMB black-body energy spectrum. Using measurements of the Deuterium and Helium-4 abundances, as well as the COBE-FIRAS constraint on μ-type spectral distortions, stringent constraints on the gravitino superWIMP parameter space can be set for NLSP lifetimes in the range $t_{\rm NLSP} \sim 10^4 - 10^8$ s. Similar considerations have also been applied to the axino superWIMP scenario, wherein a frozen-out neutralino or stau decays to an axino accompanied by an SM particle [10,11,24–27,36,37]. Independently of whether a particular axion-axino superfield realisation solves the strong CP problem, if the axino is the LSP, cosmological data can be expected to constrain a large part of the parameter space.

In this work, we extend these early analyses to include constraints from the CMB temperature and polarisation anisotropies from the *Planck* CMB mission [38]. Just as they impact on the light elements and the CMB energy spectrum, electromagnetic energy injections from NLSP decay can likewise have drastic consequences for the reionisation history of the Universe. Energy injection over NLSP lifetimes of $t_{\rm NLSP} \sim 10^{10}$–$10^{24}$ s, in particular, can significantly modify the evolution of the free-electron fraction in the cosmic plasma, altering the CMB anisotropies in ways that are strongly disfavoured by current anisotropy measurements [38,39]. As we shall demonstrate, this in turn allows us to place stringent constraints on large swathes of superWIMP parameter space previously considered viable, providing a powerful complement to conventional SUSY dark matter searches at colliders as well as at direct and indirect dark matter detection experiments.[3]

The paper is organised as follows. We begin in Sect. 2 with a summary of some well-motivated SUSY superWIMP scenarios amenable to the observational and experimental constraints of this work. In Sect. 3 we describe how these

[1] The mechanics of this production depends on the nature of the neutralino. For a light neutralino $\chi_1^0 \lesssim 100$ GeV, one requires a bino-like neutralino to have enough annihilations to avoid overclosing the Universe [14,15].

[2] This statement assumes the neutralino χ_1^0 has not been ruled out by prompt jets/leptons + missing energy searches at the LHC. Within the general 19-parameter phenomenological MSSM (PMSSM) scenario [32], large regions of the parameter space are unconstrained [33]. This is discussed in more detail in Sect. 2.

[3] We note that, in the recent years, several works have also invoked late-decaying dark matter to explain cosmological anomalies such as the Hubble and the σ_8 tensions [40–42]. Most of these scenarios do not generate significant electromagnetic emissions and are thus not subject energy injection constraints. The dominant constraints applicable to these scenarios arise from free-streaming effects and/or radiation excess (i.e., a non-standard $N_{\rm eff}$ relative to the Standard-Model prediction of $N_{\rm eff}^{\rm SM} = 3.0440 \pm 0.0002$ [43–46].

constraints can be applied to derive limits on the superWIMP parameter space, starting with cosmological observations and concluding with collider searches. Sect. 4 summarises the limits thus derived on the gravitino and axino superWIMP parameter space, assuming the initial NLSP abundance matches the observed DM abundance. We conclude in Sect. 5. Appendix Aoutlines the derivation of the LSP momentum distribution expected from NLSP-to-LSP decay, while Appendices B and C discuss scenarios in which the NLSP population is under- or over-produced.

2 SUSY superWIMPs

The general mechanism of superWIMP production in the early Universe is straightforward. Heavier SUSY particles undergo cascade decays to lighter SUSY particles and eventually to the NLSP. The NLSP then freezes out, typically at $x_{\rm f} \equiv m_{\rm NLSP}/T \sim 25$–$30$, with a yield $Y_{\rm NLSP} \equiv n_{\rm NLSP}/s$, where $n_{\rm NLSP}$ is the NLSP number density and s is the entropy. Long after freeze-out, the NLSP decays to the LSP. Assuming the decay is complete, $Y_{\rm LSP} \simeq Y_{\rm NLSP}$, and the final LSP abundance is simply given by $\Omega_{\rm LSP}h^2 \simeq (m_{\rm LSP}/m_{\rm NLSP})\,\Omega_{\rm NLSP}h^2$, where h is the reduced Hubble parameter. In most superWIMP scenarios, $m_{\rm NLSP} \simeq m_{\rm LSP}$, such that LSP inherits the same abundance as the NLSP. A large mass difference is however not precluded and can be a means to relax constraints on the LSP parameter space from relic density considerations.

For SUSY superWIMPs, if there exists a thermal production mechanism in the early Universe generating an abundance proportional to the reheating temperature, then the total superWIMP abundance today is simply the sum of the thermal population and the population arising from NLSP decay ("non-thermal"), i.e.,

$$\Omega_{\rm LSP}h^2 = \Omega_{\rm LSP}^{\rm thermal}h^2 + \Omega_{\rm LSP}^{\rm non-thermal}h^2. \tag{1}$$

In general, however, to generate by thermal means a GeV-to-TeV-mass SUSY superWIMP population to match the observed dark matter abundance requires a reheating temperature in excess of $T_{\rm rh} \sim 10^{10}$ GeV [13]. Thus, if the reheating temperature turns out to be low, the production of a sizeable population of superWIMP relics must rely entirely on NLSP-to-LSP decay. For axinos in the mass range $\mathcal{O}(\text{MeV} - \text{GeV})$, thermal scatterings can account for the correct relic density for reheating temperatures (T_{rh}) of about 10^4 GeV or lower [10].[4]

At this stage it is important to emphasise that, within the general Minimal Supersymmetric Standard Model (MSSM), the mechanism of thermal neutralino freeze-out that generates the right relic abundance is quite restricted given collider and electroweak precision observables, as well as constraints on the Higgs and Z-boson invisible widths [14,15,48–51]. The mechanism of thermal freeze-out for a relic neutralino depends on the nature of the gauge composition of the neutralino; for a comprehensive recent summary, see, e.g., [15]. If the neutralino is light, i.e., $m_{\chi_1^0} \lesssim 100$ GeV, limits on the charged components of the neutralino sector demand that the light neutral component χ_1^0 be predominantly bino.

Then, imposing the *Planck*-inferred dark matter density, $\Omega_{\rm DM}h^2 \lesssim 0.12$ [38], on the neutral relic density leads immediately to a lower limit of $m_{\chi_1^0} \gtrsim 34$ GeV on the neutralino mass [14]. Note however that for a decaying neutralino the lower limit is relaxed due to the dilution of the relic abundance. The precise lower limit will depend on the amount of dilution, along with the underlying mechanism and abundance of the relic neutralino. We use this bound as an indicative limit, but do not strictly enforce it. Thus, on the light neutralino side, assuming a thermal freeze-out mechanism the two places with maximally efficient enhancements in the annihilation cross-section so as not to overclose the Universe are at the Z-funnel and the Higgs funnel regions [14].[5] For a predominantly bino LSP, the cross-section σ for annihilation for light neutralinos to fermions f for the Higgs/Z funnel region is given by

$$\sigma(s)_{\chi_1^0\chi_1^0 \to f\bar{f}} \simeq \frac{N^2_{\chi_1^0 - Z/h}}{m_{Z/h}}\sqrt{1 - \frac{4m^2_{\chi_1^0}}{s}} \times \frac{s\Gamma_{Z/h}}{(s - m^2_{Z/h})^2 + (m_{h/Z}\Gamma_{Z/h})^2}, \tag{2}$$

where s represents the centre-of-mass energy, $m_{Z/h}$ the mass the Z/h boson, $\Gamma_{Z/h}$ the partial width of Z/h boson to fermions, and $N_{\chi_1^0 - Z/h}$ denotes the coupling of neutralinos to Z/h bosons. Direct detection constraints however rule out a significant part of the neutralino parameter space in the 10 GeV-to-1 TeV mass range [9,14,33,53], with limits depending on the specifics of the model parameters. In general spin-independent limits from the Xenon-nT/LZ direct

[4] Production of dark matter from the decay of parent particles in thermal equillibrium with the SM bath to out-of-equillibrium LSPs (with negligible initial density) can also be occur within the freeze-in mechanism [47]. For gravitinos, it can be shown that for heavy scalar superpartners, a significant fraction of dark matter can be produced by the freeze-in from superpartners, largely independently of the reheating temperature [29]. A significant part of this parameter space is however constrained by LHC collider searches for superparticles. Axino freeze-in has been considered recently in [28] for Higgsino dark matter and for an axion decay constant $f_a \sim 10^8$–10^{12} GeV in modified cosmological scenarios, with consequences for collider searches.

[5] This rather stringent condition on the neutralino mass can be relaxed within the next-to-Minimal Supersymmetric Standard Model (NMSSM), where the presence of additional scalars ensure an efficient annihilation [52]. Alternatively, a non-thermal neutralino will also ensure that these limits are significantly weakened [14].

detection experiments [49] are quite constraining in the light dark matter scenario ($m_{\chi_1^0} \lesssim 200$ GeV), leaving viable the Z/H funnel regions.[6]

At higher masses, depending on the gauge content of the neutralino and the SUSY mass spectrum, a variety of new annihilation mechanisms can open up. Given the strong limits from collider searches, the most promising scenarios proceed through co-annihilations with sleptons and squarks. If light staus $\tilde{\tau}$ or stops $\tilde{t}$ appear in the t-channel, the annihilation cross-section for a predominantly bino neutralino scale as

$$\sigma(s)_{(\chi_1^0\chi_1^0 \to f\bar{f})} \simeq \frac{g_W^4 s}{64\pi m^2_{\tilde{t}(\tilde{\tau})}}, \tag{3}$$

where $g_W = (8/\sqrt{2})G_F m_W^2$, with Fermi constant G_F and W-boson mass m_W.) In this case, co-annihilations aided by Sommerfeld enhancements can lead to the correct relic density [9,54].

We also add that if the neutralino has a sizable Higgsino component, a TeV scale Higgsino can generate the relic abundance of the Universe through co-annihilation with nearly mass-degenerate charginos [55]; this scenario requires the so-called "well-tempered" neutralino, a right admixture of bino and Higgsino for efficient annihilation [55,56]. Since the charginos are TeV scale electroweak gauginos, collider limits can be evaded if the rest of the SUSY spectrum is decoupled as in the Split SUSY cases [57]. These considerations are generally encoded within the idea of the so-called relic neutralino surface [9]. General phenomenological and simplified MSSM model studies for the electroweakino sector using LHC data have shown that large swathes of parameter space are allowed within the gaugino sector, implying that there is no generic model-independent lower bound on the light neutralino [33]. The situation is relaxed further in non-minimal models like the next-to-Minimal Supersymmetric Standard Model (NMSSM) or non-universal Gaugino Models (NUGM).

Lastly, we note that, in models with over-abundant dark matter (e.g., models involving a light bino-like neutralino), the superWIMP mechanism is a way to dilute the final relic abundance. We emphasise, however, that, unless otherwise specified, our assumption throughout the present analysis is that the NLSP is always produced with the correct relic abundance prior to decay. That is, had the NLSP been stable, its present-day reduced energy density would be equal to $\Omega_{\rm DM}$. This assumption also implies that, in those scenarios where a large mass gap exists between the NLSP and the LSP, the latter would constitute only a fraction of the observed dark matter today; the remainder would have to be explained by some other physics.

In what follows, we briefly describe two well-motivated SUSY superWIMPs, the gravitino $\tilde{G}$ and the axino $\tilde{a}$. As we shall see in Sect. 4, irrespective of the freeze-out/freeze-in mechanism that produces the NLSP neutralino, energy injection constraints of PMSSM and BBN, coupled with free-streaming bounds from the Lyα data will constrain the bulk of their parameter spaces.

2.1 Gravitino superWIMPs

Gravitinos $\tilde{G}$ are spin-3/2 superpartners of gravitons. Depending on the SUSY breaking mechanism, the gravitino mass – given approximately by $m_{\tilde{G}} \simeq \langle F\rangle/m_{\rm pl}$, where $\langle F\rangle$ is the SUSY breaking scale – can range from keV to TeV and is thus essentially a free parameter in this study. Because interactions of the gravitino are $m_{\rm Pl}$-suppressed, we do not expect them to be efficiently produced via scattering in the early Universe unless the reheating temperature is high [13].

Production from NLSP decay can proceed via the decay of the lightest neutralino χ_1^0. Stringent BBN constraints on hadronic energy injection from the decays $\chi_1^0 \to \tilde{G}h/Z$ essentially rules out a predominantly wino- or Higgsino-like neutralino [6,16]. Then, what remains is a bino-like neutralino, which decays into a gravitino predominantly via the two-body decay $\chi_1^0 \to \tilde{G}\gamma$, whose width is given by [6]

$$\Gamma(\chi_1^0 \to \tilde{G}\gamma) = \frac{m^5_{\chi_1^0}\cos^2\theta_{\rm W}}{48\pi m^2_{\rm Pl} m^2_{\tilde{G}}}\left(1-\frac{m^2_{\tilde{G}}}{m^2_{\chi_1^0}}\right)^3\left(1+3\frac{m^2_{\tilde{G}}}{m^2_{\chi_1^0}}\right), \tag{4}$$

where m_{Pl} is the reduced Planck mass, and $\theta_{\rm W}$ is the weak mixing angle.

Assuming decay at rest and that the energy carried by the photon, $E_\gamma = (m^2_{\chi_1^0} - m^2_{\tilde{G}})/(2m_{\chi_1^0})$, is injected entirely into the cosmic plasma, it is convenient to recast the width (4) as

$$\begin{aligned}\Gamma(\chi_1^0 \to \tilde{G}\gamma) &= \frac{m^3_{\chi_1^0}\cos^2\theta_{\rm W}}{3\pi m^2_{\rm Pl}}\epsilon^3_{\rm em}\frac{2-3\epsilon_{\rm em}}{1-2\epsilon_{\rm em}} \\ &\simeq 2.2\times 10^{-14}\ {\rm s}^{-1}\,\epsilon^3_{\rm em}\frac{2-3\epsilon_{\rm em}}{1-2\epsilon_{\rm em}}\left(\frac{m_{\chi_1^0}}{\rm GeV}\right)^3,\end{aligned} \tag{5}$$

with

$$\epsilon_{\rm em} \equiv \frac{E_\gamma}{m_{\chi_1^0}} = \frac{m^2_{\chi_1^0} - m^2_{\tilde{G}}}{2m^2_{\chi_1^0}} \tag{6}$$

denoting the fraction of the neutralino mass released as electromagnetic energy. Where kinematically allowed, the additional decay channels $\chi_1^0 \to \tilde{G}Z/h$ are also available. But,

[6] The limits are sensitive to the Higgsino mass parameter μ. While the $\mu > 0$ parameter space is severely restricted, constraints on $\mu < 0$ are not as restrictive [14,49].

as said above, these channels are suppressed for a bino-like χ_1^0. Note that maximal energy injection is represented by $\epsilon_{\rm em} \to 0.5$, which occurs as $m_{\tilde{G}} \to 0$. [7]

2.2 Axino superWIMPs

Axinos $\tilde{a}$ are the supersymmetric partners of the axion – the dynamic field expected to solve the strong CP problem – and appear in the axion supermultiplet after the Peccei-Quinn (PQ) symmetry breaking in the form $A = (s + ia)/\sqrt{2} + \sqrt{2}\theta a + \theta^2 F$, where a is the axion, s the saxion,[8] F the auxiliary superfield, and θ is the Grassmanian coordinate. The axion couples derivatively to quarks and to the gauge bosons with interactions suppressed by the PQ breaking scale f_a; the accompanying SUSY interactions can be found by simply supersymmetrising the effective SM-axion interactions, i.e., the axion supermultiplet A couples to the vector supermultiplet V_a. The axion supermultiplet acquires a mass after SUSY is broken. While the saxion mass is roughly set by the the soft SUSY breaking scale, the axino mass depends on the superpotential. For the purposes of this work, we will take the axino mass to be a free parameter, and note that its mass can range from eV to TeV scales.

Like gravitinos, axinos can be produced in the early Universe in abundance via thermal scattering if the reheating temperature is large [59]. However, if the axino is the LSP, production from the decay of a NLSP neutralino population is also possible. Assuming a (pure) bino decay, the decay width is given by [11,12]

$$\begin{aligned}\Gamma\left(\chi_1^0 \to \tilde{a}\gamma\right) &= \left(\frac{\alpha^2}{4\pi}\right) C_{aYY}^2 \frac{m_{\chi_1^0}^3}{4\pi^2 f_a'^2 \cos^2\theta_{\rm W}} \epsilon_{\rm em}^3 \\ &\simeq 2.1 \times 10^{-15}\ {\rm s}^{-1} \\ &\quad \times C_{aYY}^2 \epsilon_{\rm em}^3 \left(\frac{m_{\chi_1^0}}{\rm GeV}\right)^3 \left(\frac{\rm GeV}{f_a'/10^{16}}\right)^2 .\end{aligned} \tag{7}$$

Here, $f_a' \equiv f_a/N$, where the factor $N = 1$ and $N = 6$ applies to the KSVZ and DFSZ axion, respectively; the coefficient C_{aYY} is a model-dependent $\mathcal{O}(1)$ number [11], which we set to unity in this analysis without loss of generality; and $\epsilon_{\rm em}$ is given by Eq. (6), but with the replacement $m_{\tilde{G}} \to m_{\tilde{a}}$. Precision cosmology currently limits the PQ breaking scale to $f_a \gtrsim 10^8$ GeV (via the axion hot dark matter fraction) for all axion models, while the DFSZ axion is further subject to red-giant constraints on the axion-electron coupling, such that $f_a \gtrsim 10^{10}$ GeV [60]. Note also that for $f_a \gtrsim 10^{12}$, the axion can contribute significantly to the observed dark matter abundance of the Universe.[9]

As in the case of the χ_1^0 decay to gravitino, where kinematically viable, the decay $\chi_1^0 \to \tilde{a}Z$ is also allowed albeit suppressed relative to $\chi_1^0 \to \tilde{a}\gamma$ in both the decay width and the accompanying electromagnetic energy release. The possibility also exists that the gravitino (axino) is the NLSP and decays into the axino (gravitino) LSP accompanied by the release of an axion: this process has in fact been claimed to solve the Hubble tension through the injection of dark radiation [42].

3 Cosmological and collider probes of superWIMPs

From the cosmological perspective, the two defining features of superWIMPs are (i) the NLSP decays to the LSP on cosmological time scales, and (ii) the decay is accompanied by the release of electromagnetic radiation. Irrespective of whether the NLSP or LSP accounts for the entirety of the observed dark matter abundance, these features can manifest themselves in precision cosmological observables either via the electromagnetic radiation or in the kinematic properties of the LSP itself. We elaborate on the relevant cosmological observables and how they can be used to constrain superWIMPs in the following subsections. For completeness, we also discuss collider probes of superWIMPs in Sect. 3.5.

3.1 Light element abundances

The main effect of electromagnetic energy injection into the plasma on the abundances of the light elements (Deuterium ^{2}H, Helium-3 ^{3}He, and Helium-4 ^{4}He) from BBN is photo-dissociation, provided that the injected energy exceeds the reaction threshold (typically $\mathcal{O}$(2–30) MeV; see, e.g., Table 1 of Ref. [61]). However, the energy fraction available for photo-dissociation is strongly suppressed if the injection occurs when the plasma temperature is above $T \sim 10$ keV (or, equivalently, $t \sim 10^4$ s). This is because, at these plasma temperatures, energy injections that exceed even the lowest photo-dissociation thresholds will also exceed the threshold for pair production ($\gamma\gamma \to e^+e^-$), $E_c \simeq m_e^2/(22T)$ [62,63]. Given that CMB photons outnumber baryons by a factor of 10^9, pair production must dominate over all other

[7] The limit $m_{\tilde{G}} = 0$ is ill-defined within theories of SUSY breaking mechanisms. Since $m_{\tilde{G}}$ is related to the SUSY breaking scale $\langle F \rangle$, the $\langle F \rangle \to 0$ limit simply means a decoupled massless gravitino. Swampland conjectures relate it to the massless limit of an infinite tower of states and the breakdown of the effective field theory [58].

[8] Although we will ignore the saxion for this work, saxions can also form superWIMPs and be subject to cosmological energy injection constraints.

[9] If the misalignment angle is $\mathcal{O}(1)$, such as in the post-inflationary scenario, then to explain the observed dark matter abundance of the Universe fixes $f_a \sim 10^{12}$ GeV. However, in the "anthropic" or pre-inflationary scenario, the misalignment angle is random; in this case there is no upper limit on f_a.

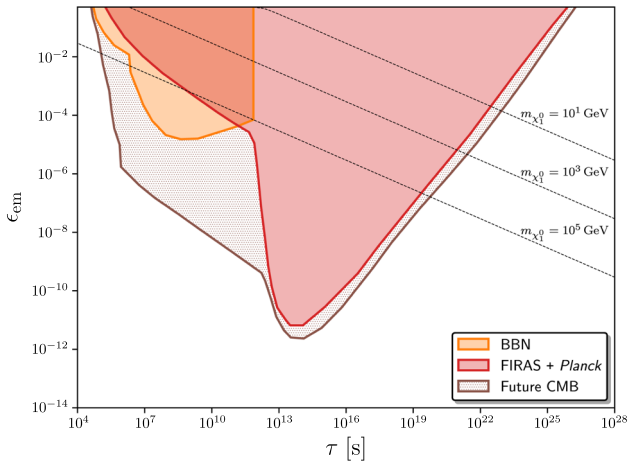

Fig. 1 Current and projected constraints on the fractional energy injection ϵ_{em} as a function of decay lifetime τ from the BBN light element abundances (H^2 and He^3), current CMB measurements (FIRAS+*Planck*), and future CMB probes (LiteBIRD+CMB-S4+PRISM). These constraints have been extracted from Fig. 8 of Ref. [39], where the exclusion limits correspond to the $\Delta\chi = 4$ isocontours on a variable fraction f_{frac} of dark matter decaying via DM $\to \gamma\gamma$ for which the fractional injection is always fixed at $\epsilon_{em} = 1$; we have reintepreted these isocontours to constraints on a variable ϵ_{em} for a fixed $f_{frac} = 1$. The mapping is to a good approximation one-to-one, provided that the initial energy injection exceeds ~ 100 MeV in the case of BBN and ~ 1 MeV in the case of CMB. To illustrate the power of these constraints, the black dashed lines indicate predictions for the gravitino superWIMP scenario, based on Eq. (5), for several neutralino mass values, assuming that the neutralino population has been produced at the correct relic abundance prior to decay

electromagnetic processes whenever kinematically allowed, and quickly degrade the injected energy to below the photodissociation threshold. For this reason, as a tool for constraining electromagnetic energy injection from particle decay, the light element abundances are sensitive only to decay lifetimes longer than $\tau \sim 10^4$ s.

Figure 1 shows the region on the (τ, ϵ_{em})-plane excluded by the ^{2}H and ^{3}He abundances (shaded orange). These constraints have been extracted from Fig. 8 of Ref. [39], itself based on Ref. [64]'s adaption of Ref. [65]'s results, for initial energy injections larger than ~ 100 MeV. Note that Ref. [39] had presented their results in the form of constraints on a variable f_{frac} as a function of the decay lifetime τ, where f_{frac} is the fraction of dark matter that decays via DM $\to \gamma\gamma$, i.e., the fractional energy injection is fixed at $\epsilon_{em} = 1$. In Fig. 1 we have reinterpreted these constraints to be upper limits on the fractional energy injection ϵ_{em} at a fixed $f_{frac} = 1$, assuming that the decaying NLSP population has been produced with the correct relic abundance prior to decay. The reintepretation should to a good approximation be one-to-one, provided that, for the light element abundances, the initial energy injection always respects $\gtrsim 100$ MeV. For sub-100 MeV injections, bounds on f_{frac} or ϵ_{em} are strongly dependent on the initial energy injection [61,66,67], making this mapping less straightforward. The hard cut-off of the BBN limits at $\tau \simeq 10^{12}$ s in the figure is simply due to the lack of calculations in this parameter region in the literature; we are otherwise not aware of any fundamental reason why BBN constraints could not be extended to longer decay lifetimes.

To illustrate the power of energy injection constraints, we have also plotted in Fig. 1 predictions for the gravitino superWIMP scenario, based on Eq. (5), for a number of χ_1^0 masses from $m_{\chi_1^0} = 1$ GeV and up to the unitarity limit of $m_{\chi_1^0} = 100$ TeV.[10] We note however that the unitarity bound is indicative, since the bound will be relaxed due to the decaying neutralino. We emphasise that for a given mass hierarchy between the neutralino and the gravitino, the amount of energy released and the lifetime are fixed by Eq. (5). That is, there are no further variables that can affect the gravitino superWIMP predictions in Fig. 1. As mentioned earlier, the maximal fractional energy released can never be exactly equal to 0.5, which would correspond to a massless gravitino.

3.2 CMB spectral distortions

Electromagnetic energy injection in the early Universe must also perturb the Planck blackbody energy spectrum of the CMB photons, creating a spectral distortion. If both photon number-changing processes, (e.g., double Compton scattering and Bremsstrahlung) and energy-changing processes (e.g., Compton scattering) occur efficiently, then these distortions are quickly wiped out, leaving no trace of the decay in the CMB energy spectrum besides a temperature shift (which is unobservable by spectral measurements, but may be detectable in the anisotropies via N_{eff}). However, should these processes be inefficient at the time of energy injection and remain inefficient until the present time, the spectral distortions they cause may freeze in and become observable.

A detailed review of CMB spectral distortions can be found in, e.g., [69,70]. As a rule of thumb, energy injections at redshifts $z \gtrsim 2 \times 10^6$ generally do not survive to be detected as spectral distortions, as the aforementioned photon number- and energy-changing processes are extremely effective at their erasure. When the redshift drops below $z \sim 2 \times 10^6$, double Compton and Bremsstrahlung begin to abate, while Compton scattering continues to redistribute the photon energy with efficiency. Under these conditions, exotic energy injection will generally result in a Bose–Einstein

[10] The unitarity limit quoted here comes from Ref. [68], which argues as follows: in order for the neutralino to not exceed the upper limit on the relic abundance, the velocity-averaged cross-section must satisfy $\langle\sigma v\rangle \gtrsim 3\times10^{-26}\,\mathrm{cm^3\,s^{-1}}$. For an s-wave annihilation with perturbative couplings, this imposes an upper limit on the neutralino mass of $m_{\chi_1^0} \lesssim$ 30–100 TeV, depending on the nature of the interaction. We take $m_{\chi_1^0} \lesssim$ 100 TeV as a conservative limit.

energy spectrum with a chemical potential μ; such a deviation from the Planck spectrum is also called a μ-distortion.

As the Universe evolves to $z \lesssim 10^4$, Compton scattering too becomes inefficient; at these times, the primary effect of photon scattering on hot electrons is to shift the low-energy photons in the Rayleigh–Jeans part of the spectrum to the high-energy Wien tail (i.e., upscattering). Thus, exotic energy injection at these times will not be redistributed to an equilibrium form, but instead results in a so-called y-distortion to the Planck spectrum whose shape is distinct from that of a chemical potential μ. In other words, the exact shape of the spectral distortion contains in principle some amount of information on the time of the energy injection, with a pure μ- and pure y-distortion representing respectively the early and the late extremes. We note however that while a μ-distortion is uniquely associated with energy injections in the early Universe, astrophysics at low redshifts, e.g., the Sunyaev–Zeldovich effect at $z \lesssim 20$, can also produce y-distortions that are typically much larger than what can be expected from distortions at pre-recombination times. Although this does not prevent us from using null measurements of y-distortion to set constraints on early exotic energy injection scenarios, a positive measurement may not necessarily signal new particle physics.

Measurements of the CMB energy spectrum by the FIRAS instrument aboard COBE currently limits μ-type and y-type distortions to $|\mu| \lesssim 9 \times 10^{-5}$ and $|y| \lesssim 1.5 \times 10^{-5}$ (95% C.L.), respectively [71,72]. On the $(\tau, \epsilon_{\rm em})$-plane in Fig. 1, these limits are primarily responsible for constraining the $\tau \lesssim 10^{13}$ s section of the FIRAS+*Planck* exclusion region (shaded red). [11] A PRISM-like spectral measurement in the future could improve the sensitivity to $\delta\mu \sim 9\times10^{-10}(2\sigma)$ [39,73], and is the main reason behind the improved constraints on $\epsilon_{\rm em}$ anticipated from future CMB experiments (shaded brown) at $\tau \lesssim 10^{12}$ s.

3.3 CMB anisotropies

At $t \gtrsim 10^{12}$ s, electromagnetic energy injection into the cosmic plasma also begins to interfere with the atoms (mostly Hydrogen) in the Universe in an observable way via ionisation, excitation, and heating. This interference modifies directly the evolution of the free electron fraction – and hence how transparent the Universe is to photons – and has strong manifestations in the CMB temperature and polarisation anisotropies. Energy injection around the time of CMB formation ($t \sim 10^{13}$ s) has a particularly strong impact, as it would delay recombination, thereby enhancing Silk damping and hence leading to a suppressed temperature-temperature angular power spectrum on small scales; it is to these timescales that the CMB anisotropies are maximally sensitive to energy injection. Recombination itself is not affected if the energy injection occurs at a later time $t \gg 10^{-13}$ s. Nonetheless, increased ionisation of the intergalactic medium between the epochs of recombination ($z \sim 1100$) and reionisation ($z \sim 10$) raises the optical depth, which manifests itself most prominently in a stronger E-polarisation signal at multipoles $\ell \sim 20$ [67].

On the $(\tau, \epsilon_{\rm em})$-plane shown in Fig. 1, constraints from the *Planck* measurements of the CMB anisotropies are primarily responsible for $\tau \gtrsim 10^{13}$ s part of the FIRAS+*Planck* exclusion region (shaded red). In the future, the combination of LiteBIRD+CMB-S4+PRISM (shaded brown) can be expected to improve upon existing constraints. However, as can be seen Fig. 1 and also discussed above in Sect. 3.2, the largest improvement over current CMB constraints on $\epsilon_{\rm em}$ pertains to shorter decay lifetimes $\tau \lesssim 10^{12}$ s and is due mainly to better spectral distortion measurements from a PRISM-like instrument; the improvement on the $\epsilon_{\rm em}$ constraints expected for longer lifetimes $\tau \gtrsim 10^{13}$ s from future CMB anisotropy measurements is relatively modest.

Lastly, we note again that our $\epsilon_{\rm em}$ constraints from the CMB have been mapped from the $f_{\rm frac}$ constraints of Ref. [39]. This mapping is direct, provided that the energy injection exceeds ~ 1 MeV and that the energy is deposited in the plasma instantly upon injection.

3.4 Lyman-α forest

The production of superWIMPs via NLSP-to-LSP decay is always accompanied by a finite momentum for the LSP, given at the production time $t_{\rm prod}$ by $p_{\rm LSP}(t_{\rm prod}) = p_\star = (m^2_{\chi_1^0} - m^2_{\rm LSP})/(2m_{\chi_1^0}) = \epsilon_{\rm em} m_{\chi_1^0}$, assuming decay at rest. Universal expansion causes $p_{\rm LSP}$ to redshift subsequently as $p_{\rm LSP}(t) = p_\star R_{\rm prod}/R(t)$, where $R(t)$ is the scale factor and $R_{\rm prod} \equiv R(t_{\rm prod})$; at a later time t the corresponding LSP velocity therefore reads

$$v_{\rm LSP}(t) = \frac{p_\star}{\sqrt{p_\star^2 + m^2_{\rm LSP} R^2(t)/R^2_{\rm prod}}} = \frac{1}{\sqrt{1 + R^2(t)/v_0^2}}, \tag{8}$$

where

$$v_0 \equiv \epsilon_{\rm em} \frac{m_{\chi_1^0}}{m_{\rm LSP}} R_{\rm prod} = \frac{\epsilon_{\rm em}}{\sqrt{1-2\epsilon_{\rm em}}} R_{\rm prod} \tag{9}$$

is the present-day ($R(t_0) = 1$) LSP velocity, under the assumption that $m_{\rm LSP} \gg p_{\rm LSP}(t_0)$ holds.

Because the NLSP-to-LSP decay is isotropic, the overall effect of a finite $v_{\rm LSP}$ is that of isotropic LSP free-streaming. Furthermore, because NLSP-to-LSP decay is a continuous

[11] The analysis of Ref. [39], on which Fig. 1 is based, in fact used the full energy spectrum measurement from FIRAS (i.e., not just derived limits on the μ and y parameters) to put constraints on the $(\tau, f_{\rm frac})$-plane.

process, together with a redshifting $p_{\rm LSP}$ we can expect a present-day comoving LSP number density $n_{\rm LSP}(t_0)$ to be composed of a distribution of particles in momentum space, given approximately by

$$n_{\rm LSP}(t_0) \simeq \frac{\Omega_{\rm DM}\rho_{\rm crit}}{m_{\chi_1^0}} \times \left\{ 2\int_0^{p_\star R_{\rm eq}} {\rm d}\ln p \left(\frac{p}{p_\star R_\Gamma}\right)^2 \exp\left[-\left(\frac{p}{p_\star R_\Gamma}\right)^2\right] + \frac{3}{2}\int_{p_\star R_{\rm eq}}^{p_\star} {\rm d}\ln p \left(\frac{p}{p_\star R_\Gamma}\right)^{3/2} \exp\left[-\left(\frac{p}{p_\star R_\Gamma}\right)^{3/2}\right] \right\}, \tag{10}$$

where the prefactor assumes the χ_1^0 population was produced with the correct relic abundance, R_Γ is the scale factor corresponding to NLSP lifetime $t = \tau \equiv 1/\Gamma$, and $R_{\rm eq}$ is the scale factor at matter-radiation equality. See Appendix A for the derivation of Eq. (10). Thus, phenomenologically, the LSP population today is dispersive and akin to a warm dark matter (WDM) with a present-day characteristic velocity given approximately by $v_0 \sim p_\star R_\Gamma / m_{\rm LSP}$. This also means that limits on thermal WDM properties from small-scale fluctuation measurements such as the Lyman-α forest can be reinterpreted to constrain properties of the LSP and the corresponding superWIMP parameter space [74].

Several recent studies have investigated how to map thermal WDM bounds from the Lyman-α forest to constraints on WDM from particle decays, e.g., [75,76]. Roughly, one would compute the linear transfer function of the WDM given the daughter particle's phase space distribution, and match it to the thermal WDM transfer function that exhibits free-streaming suppression at approximately the same location in wave number k. Here, however, we adopt the simpler approach of estimating the comoving particle horizon – also called the free-streaming horizon – of the LSP population.

The free-streaming horizon arises naturally in semi-analytical solutions of the Vlasov equation that governs the evolution of the linear transfer function. Its inverse correlates with the location in k-space of power suppression due to free-streaming, and can therefore be seen as a proxy for the transfer function. For a LSP produced at a fixed time $t_{\rm prod}$ and observed later at a time $t_{\rm obs}$, the free-streaming horizon is given by

$$\lambda_{\rm FS}(t_{\rm obs}, t_{\rm prod}) = \int_{t_{\rm prod}}^{t_{\rm obs}} \frac{{\rm d}t}{R(t)} v_{\rm LSP}(t) = \int_{R_{\rm prod}}^{R_{\rm obs}} \frac{{\rm d}R}{R^2 H(R)} v_{\rm LSP}(R), \tag{11}$$

where $t_{\rm obs}$ corresponds typically to a low redshift of $z \sim 2$, $t_{\rm prod}$ to some time prior to matter-radiation equality, and $H \equiv (1/R)({\rm d}R/{\rm d}t)$ is the Hubble expansion rate. Because NLSP decay is a continuous process, in principle we must calculate $\lambda_{\rm FS}$ for all possible production times $t_{\rm prod}$ and then average it over the momentum distribution of Eq. (10). For simplicity, however, we assume all LSPs to be produced at $t_{\rm prod} = 1/\Gamma$; this is a reasonable approximation given that, as shown in Eq. (10), LSPs produced at $t_{\rm prod} \sim 1/\Gamma$ – whose characteristic momentum is $\sim p_\star R_\Gamma$ – in any case dominate the LSP distribution today. Then, using Eq. (8) and setting $t_{\rm prod} = 1/\Gamma$, Eq. (11) can now be rewritten as

$$\begin{aligned}\lambda_{\rm FS}(R_{\rm obs}, R_\Gamma) &= \frac{1}{H_0}\sqrt{\frac{R_{\rm eq}}{\Omega_{\rm m}}} \int_{R_\Gamma/R_{\rm eq}}^{R_{\rm obs}/R_{\rm eq}} \frac{{\rm d}y}{\sqrt{(1+y)[1+(R_{\rm eq}/v_0)^2 y^2]}} \\ &\simeq 91\, h^{-1}{\rm Mpc} \sqrt{\left(\frac{3401}{1+z_{\rm eq}}\right)\left(\frac{0.32}{\Omega_{\rm m}}\right)} \\ &\quad \times \int_{R_\Gamma/R_{\rm eq}}^{R_{\rm obs}/R_{\rm eq}} \frac{{\rm d}y}{\sqrt{(1+y)[1+(R_{\rm eq}/v_0)^2 y^2]}},\end{aligned} \tag{12}$$

valid across the radiation and matter domination epochs, where the subscript "eq" denotes matter-radiation equality, $\Omega_{\rm m}$ is the present-day reduced total matter density, and h is the reduced Hubble parameter defined via $H_0 = 100\, h$ km s^{-1} Mpc^{-1}.

The typical Lyα WDM bound in the literature is presented as a lower limit on the WDM mass $m_{\rm WDM}$, assuming that the WDM constitutes the entirety of the dark matter abundance of the Universe and that the WDM population follows a relativistic Fermi-Dirac distribution, with a temperature linked to the dark matter abundance, i.e.,

$$\Omega_{\rm WDM}h^2 = \left(\frac{T_{\rm WDM}}{T_\nu}\right)^3 \left(\frac{m_{\rm WDM}}{94\ {\rm eV}}\right), \tag{13}$$

where T_ν is the temperature of the neutrino background ($T_{\nu,0} = 1.95$ K). Fixing $\Omega_{\rm WDM}h^2 = 0.12$ and using the current best limit $m_{\rm WDM} \gtrsim 5.3$ keV (95% C.I.) [77], we find an upper bound on the present-day WDM temperature of $T_{\rm WDM,0} \lesssim 2.2 \times 10^{-5}$ eV, or equivalently, a bound on the present-day average WDM velocity of $v_{\rm WDM,0} \simeq 3\, T_x/m_x \lesssim 1.2 \times 10^{-8}$. Following the steps outlined above and letting $R_{\rm prod} \to 0$, it is straightforward to show that the equivalent upper limit on the comoving WDM free-streaming horizon at $z_{\rm obs} = 2$ is

$$\lambda_{\rm FS}^{\rm WDM}(z_{\rm obs} = 2) \lesssim 0.045\, h^{-1}{\rm Mpc} \sqrt{\left(\frac{3401}{1+z_{\rm eq}}\right)\left(\frac{0.32}{\Omega_{\rm m}}\right)}. \tag{14}$$

This limit can in principle serve as an upper bound on $\lambda_{\rm FS}(z_{\rm obs} = 2, z_\Gamma)$ for those superWIMP scenarios wherein

Table 1 Upper limit on the free-streaming horizon $\lambda_{\rm FS}^{\rm WDM}$ as a function of the WDM fraction $f_{\rm WDM}$. These limits have been mapped from the two-dimensional 68%-credible contours in $(f_{\rm WDM}, m_{\rm WDM})$-plane in Fig. 12 of Ref. [79], which dates from 2009. In the comparable case of $f_{\rm WDM} = 1$, we note that the limit $m_{\rm WDM} \gtrsim 5.3$ keV (95% C.I.) quoted in the text comes from a more recent 2017 analysis [77] and translates to $\lambda_{\rm FS}^{\rm WDM} \lesssim 0.045\,h^{-1}$Mpc (see also Eq. (14)), in contrast to $\lambda_{\rm FS}^{\rm WDM} \lesssim 0.0708\,h^{-1}$Mpc tabulated below. The Lyα limits used in our analysis are therefore quite conservative

$f_{\rm WDM}$	Upper limit on $\lambda_{\rm FS}^{\rm WDM}$ $[h^{-1}$Mpc]
0.15	0.323
0.2	0.272
0.3	0.208
0.4	0.156
0.5	0.130
0.6	0.113
0.7	0.102
0.8	0.0938
0.9	0.0813
1.0	0.0708

the LSP explains *all* of the observed dark matter abundance. [12]

A more versatile analysis of the Lyα data could however also consider the possibility of a mixed cold+warm dark matter cosmology and vary as part of the fitting procedure the fraction of the total dark matter in the form of WDM, $f_{\rm WDM} \equiv \Omega_{\rm WDM}/\Omega_{\rm DM}$. Reference [79] has provided such an analysis and presented the outcome as two-dimensional constraints in the $(f_{\rm WDM}, m_{\rm WDM})$-plane and in the $(f_{\rm WDM}, v_0)$-plane (see Fig. 12 of [79]). We have translated these constraints to constraints in the $(f_{\rm WDM}, \lambda_{\rm FS}^{\rm WDM})$-plane. See a representative set in Table 1. Observe that the upper limit on $\lambda_{\rm FS}^{\rm WDM}$ deteriorates as we decrease the WDM fraction $f_{\rm WDM}$; at $f_{\rm WDM} \lesssim 0.15$, no limit can be set on $\lambda_{\rm FS}^{\rm WDM}$. In our analysis of superWIMPs, we take the WDM energy density to be $\Omega_{\rm WDM} \simeq (m_{\rm LSP}/m_{\rm NSLP})\Omega_{\rm DM}$, in accordance with our assumption that the NLSP population is always produced with the correct abundance prior to decay. It then follows simply that $f_{\rm WDM} = m_{\rm LSP}/m_{\rm NLSP}$, with the proviso that the remaining $1 - f_{\rm WDM}$ of the dark matter is cold and explained by some other physics. We apply the Lyα constraints only to those cases where production takes place before matter-radiation equality, i.e., $1/\Gamma \leq t_{\rm eq}$, because using $\lambda_{\rm FS}$ as a proxy for small-scale suppression is likely unreliable if the bulk of the NLSP decay happens deep in matter domination. [13]

3.5 Collider constraints

We assume from the outset that the neutralino is not ruled out by conventional jets/leptons + missing energy searches. In principle, within the scope of specific mass spectra, part of the parameter space can indeed be ruled out; however, this requires a larger global fit within specific simplified or full SUSY models. The GAMBIT collaboration has performed a global fit of the pMSSM within a reduced 7-parameter space – the relevant parameters being the trilinear couplings, Higgsino mass parameters, diagonal sfermion masses, and $\tan\beta$ – taking into account collider, direct detection and relic density observables [33]. They conclude that a large volume of the pMSSM parameter space remains unconstrained, with the neutralino mass ranging from the Z/H funnel region to the mulit-TeV scale. In an extended set-up that includes gravitinos, for a gravitino mass fixed at $m_{\tilde{G}} = 1$ eV, best-fit points that take into account collider searches for the rest of the electroweak gaugino sector indicate that both light and heavy neutralinos remain unconstrained within a variety of simplified-model scenarios [80]. Scenarios like split SUSY models [57,81] also predict mass spectra that are unconstrained by LHC searches. Thus, we re-emphasize that collider bounds on neutralinos are model independent and depends on the specifics of the mass spectrum and neutralino composition.

Bearing the above in mind, we summarise in this subsection collider constraints on the gravitino and the axino LSP originating from neutralino decay. The neutralino proper decay length to gravitino can be expressed following Eq. (5) as a function of the fractional energy $\epsilon_{\rm em}$ and the neutralino mass $m_{\chi_1^0}$:

$$L = c\tau \simeq 1.4 \times 10^{22}\ {\rm m}\ \frac{1-2\epsilon_{\rm em}}{\epsilon_{\rm em}^3(2-3\epsilon_{\rm em})}\left(\frac{\rm GeV}{m_{\chi_1^0}}\right)^3 . \qquad (15)$$

Collider searches – including searches of prompt decays that occur at the interaction vertex and are hence sensitive to pho-

[12] Constraints on the free-streaming properties of the dark matter can also be derived from the distribution of Milky Way satellite galaxies. Observations currently limit the thermal WDM mass to $m_{\rm WDM} \gtrsim 6.5$ keV (95% C.I.) [78] assuming $f_{\rm WDM} = 1$, marginally better than the Lyα bound of Ref. [77]. We therefore do not consider Milky Way constraints here.

[13] Since we must always compute v_0, the possibility also exists to constrain superWIMP scenarios using the thermal WDM limit on $v_{\rm WDM,0}$, instead of the more complicated $\lambda_{\rm FS}^{\rm WDM}$. Indeed, the limits in the superWIMP parameter space do turn out to be quite similar if we restrict $t_{\rm prod}$ to the radiation-domination epoch. Conceptually though, we note that v_0 describes only the instantaneous free-streaming behaviour of the LSP population, while $\lambda_{\rm FS}$ is able to capture a more complete free-streaming history; the difference between the two measures becomes more marked if LSP production takes place during matter domination. We emphasise however that neither measure is likely accurate if NLSP-to-LSP decay happens deep in the matter domination epoch, as the growth histories of the density perturbations in such scenarios – especially as the growth enters the nonlinear regime – deviate too strongly from the conventional thermal WDM scenario.

tons plus missing energy signatures, and LLP searches sensitive to delayed decays – probe proper decay lengths of about 100 m. Thus, in order for colliders to be sensitive to the gravitino superWIMP scenario, it is *a priori* clear that a large mass hierarchy must exist between the neutralino and the gravitino.

The LEP experiment has placed a lower bound on the gravitino mass from the process $e^+e^- \to \tilde{G}\tilde{G}\gamma$ of $m_{\tilde{G}} \gtrsim 1.09 \times 10^{-5}$ eV [82]. Furthermore, under the assumption that the rest of the SUSY spectrum is decoupled apart from the selectron and the neutralino χ_1^0, the LEP searches exclude a neutralino mass of up to $m_{\chi_1^0} \simeq 200$ GeV for a gravitino mass of $m_{\tilde{G}} \lesssim 10^{-5}$ eV. At the LHC, gravitino searches have been conducted within the context of gauge mediated supersymmetry (GMSB) breaking models [83]. These searches look for displaced photons assuming a SUSY topology that yields the neutralino NLSP. Assuming a decay channel with maximal production cross-section in the $pp \to \tilde{q}\tilde{q} \to qq\chi_1^0\chi_1^0$ followed by the displaced photon signature of $\chi_1^0 \to \tilde{G}\gamma$, the ATLAS experiment rules out neutralino masses in the range $\sim$ 100–400 GeV for $c\tau \sim 10$–10^4 cm [84]. The latest CMS result [85] at 13 TeV with 78 fb^{-1} luminosity excludes within these scenarios a neutralino mass in the range $m_{\chi_1^0} \sim 200$–550 GeV, for $c\tau \sim 10$–10^4 cm. We will use these experimental bounds for illustrative purposes, but emphasise that they are model-dependent.

Similar considerations apply to the axino superWIMP, in which case we have an additional degree of freedom in the neutralino decay width, namely the axion decay constant $f_a' \equiv f_a/N$. The proper decay length for the axino follows simply from Eq. (7):

$$L = c\tau \simeq 14.15 \text{ m } \epsilon_{\rm em}^{-3} \left(\frac{f_a'}{10^8 \text{ GeV}}\right)^2 \left(\frac{100 \text{ GeV}}{m_{\chi_1^0}}\right)^3 . \quad (16)$$

As with the gravitino, collider constraints on the axino superWIMP scenario depend in general on the model specifics. Independently of the specifics, however, in order for colliders to be sensitive to the parameter space, the decay length should be $\lesssim \mathcal{O}(100)$ m. Within the context of specific models, estimates have been made on the capability of the LHC to probe axinos from neutralino decays in prompt and LLP searches [28]. In this work we will reinterpret existing LLP search results to put limits on this decay process.

Finally, since we are dealing with long-lived neutralinos, if they are light (GeV/sub-GeV), there is potentially sensitivity at fixed-target experiments such as CHARM [86,87], NA62 [88], NOMAD [89], SHiP [90] and SEAQuest [91], as well as at forward physics facility experiments like FASER [30].

The production of neutralinos in fixed-target experiments depend on the specifics of the model. Typically in such experiments, a beam of particles with energies ranging from $\sim$ 100 GeV (SEAQuest) to $\sim$ 450 GeV (SHiP, NOMAD, NA62) collides with the target, thereby producing hadrons and weakly-interacting particles that could be captured in a far detector. If the rest of the SUSY spectrum is decoupled and heavy, neutralino production proceeds primarily from the decay of pseudo-scalar and vector mesons. These neutralinos then decay to gravitinos/axinos with decay widths given by Eqs. (4) and (7). Thus, the number of long-lived neutralino decays within a fixed-target experiment depends on the decay lifetime, the Lorentz boost factor, and the energy spectrum of the mesons specific to the experiment. While a full analysis for each experiment is beyond the scope of this work, a crude estimate suggests that the NOMAD experiment can exclude up to $m_{\chi_1^0} \simeq 300$ MeV for a fixed $m_{\tilde{a}} \simeq 20$ MeV, assuming $f_a \simeq 10^3$ GeV. For the same fixed value of $m_{\tilde{a}}$, a future experiment like SHiP can rule out $f_a = 10^4$ GeV for $m_{\chi_1^0} \simeq 300$ MeV.[14]

In the case of FASER, a recent assessment of its feasibility to probe light axinos and gravitinos found that, for $m_{\tilde{a}} \simeq 10$ MeV, it is possible to rule out $f_a \simeq 10^2$–10^3 GeV for $m_{\chi_1^0} \simeq 300$ MeV [93].

4 Impact of constraints on the superWIMP parameter space

Having discussed the relevant cosmological and collider probes of superWIMPs, we are now in a position to present the constraints on the gravitino and the axino superWIMP parameter spaces, assuming that the neutralino has been produced with an abundance matching the observed DM density prior to decay. These are shown in Figs. 2 and 3 in the $(m_{\chi_1^0}, m_{\rm LSP})$- and $(m_{\chi_1^0}, \epsilon_{\rm em})$-projections, highlighting respectively the hierarchical $(m_{\chi_1^0} \gg m_{\rm LSP})$ and degenerate $(m_{\chi_1^0} \simeq m_{\rm LSP})$ regions (recall that $2\epsilon_{\rm em} = \Delta m^2/m^2_{\chi_1^0}$, where $\Delta m^2 \equiv m^2_{\chi_1^0} - m^2_{\rm LSP}$ is the NLSP-LSP squared-mass gap). Detailed discussions of these results follow below. The equivalent constraints in the cases of an under- or over-production of neutralinos at 10%, 0.1%, and 10 times the observed DM abundance are presented in Appendices B and C.

4.1 Gravitino

Figure 2 shows the current and projected cosmological and collider constraints on the gravitino superWIMP parameter space in the $(m_{\chi_1^0}, m_{\tilde{G}})$-plane (left panel) and the $(m_{\chi_1^0}, \epsilon_{\rm em})$-plane (right panel). A quick glance at both reveals that a large parameter region from the hierarchical to the degenerate limit is strongly constrained by a plethora of cosmological observations. In particular, we observe that for a neutralino

[14] Also see detailed estimates provided by [92], with which we agree.

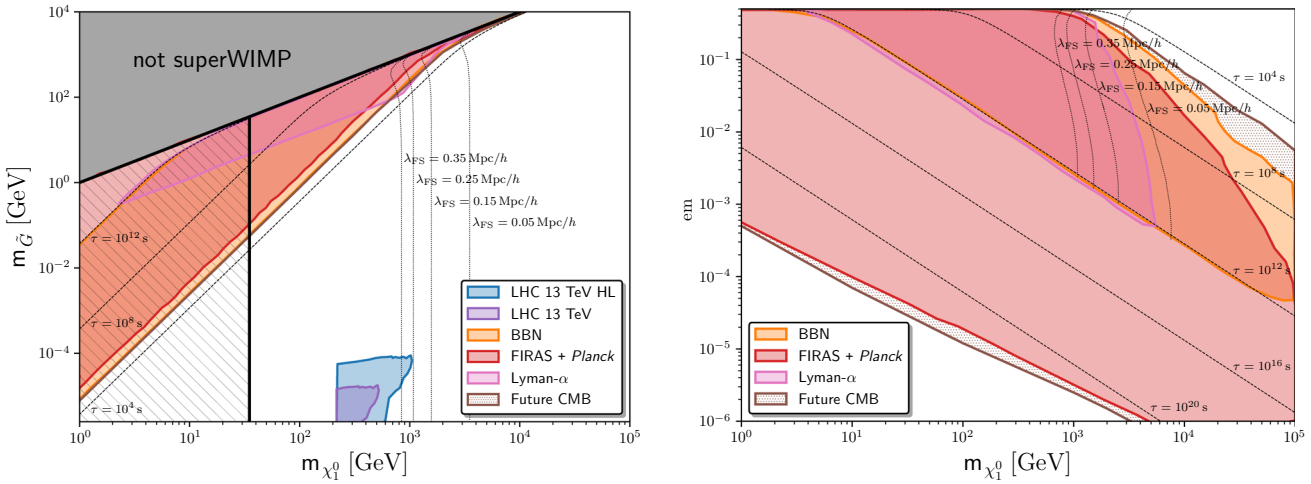

Fig. 2 Left: current and projected constraints on the gravitino superWIMP parameter space in the $(m_{\chi_1^0}, m_{\tilde{G}})$-plane. Exclusion regions labelled BBN, FIRAS+*Planck*, and FutureCMB are based on the energy injection considerations of Fig. 1. The Lyman-α constraints are derived from upper limits on the WDM free-streaming horizon as a function of the WDM fraction in Table 1. All cosmological constraints assume the neutralino population has been produced at an energy density matching the observed DM abundance prior to decay. Collider constraints from the LHC exclude the region shaded in purple, while projected constraints from HL-LHC are shown in blue. The region marked "not superWIMP" does not satisfy the superWIMP condition $m_{\chi_1^0} > m_{\tilde{G}}$, while the maximum value on the horizontal axis, $m_{\chi_1^0} = 100$ TeV, corresponds to the unitarity limit (see Footnote 10). The hatched region indicates where a neutralino abundance will overclose the Universe in the context of the freeze-out mechanism given current collider constraints on the neutralino couplings [14]; we do not however enforce this constraint, since any one of non-thermal production mechanism, late entropy injection, or modified cosmological histories could in principle weaken the exclusion limit. For clarity, we also show several lines of constant neutralino lifetime τ (black short dashed lines) and constant gravitino free-streaming horizon Λ_{FS} (black dotted lines). An additional exclusion region exists in principle between $\tau \simeq 2 \times 10^{11}$ s and 8×10^{13} s from consideration of the excess radiation energy density produced by the decay, which impacts on the expansion rate. See Appendix C for details. However, as the exclusion region is merely a sliver of the parameter space already ruled out by BBN and CMB energy injection constraints, we have chosen not to plot it. Right: Similar to the left panel, but in the $(m_{\chi_1^0}, \epsilon_{em})$-plane and without LHC constraints

mass fixed at $m_{\chi_1^0} = 100$ GeV, the totality of cosmological observations rules out gravitino masess lying in the range

$$0.8 \lesssim m_{\tilde{G}}/\mathrm{GeV} \lesssim 99.998, \tag{17}$$

while for $m_{\chi_1^0} = 1$ TeV the exclusion region lies in the range

$$270 \lesssim m_{\tilde{G}}/\mathrm{GeV} \lesssim 999.997. \tag{18}$$

As a rule of thumb, the lower end of these exclusion regions in the gravitino mass $m_{\tilde{G}}$ is driven by how *short* a neutralino lifetime τ a particular cosmological observation can probe with some precision, and is currently dominated by energy injection constraints from observations of the primordial ^{2}H and ^{3}He abundances. This limit can be seen most clearly in the left panel of Fig. 2 represented by the lower edge of the orange-shaded area at $m_{\chi_1^0} \lesssim 1$ TeV, and in the right panel by the upper edge of the orange-shaded area at $m_{\chi_1^0} \gtrsim 1$ TeV. A future CMB spectral measurement by a PRISM-like instrument will contribute to tightening the lower limit on $m_{\tilde{G}}$ primarily in the degenerate $(m_{\chi_1^0} \simeq m_{\tilde{G}})$ region at $m_{\chi_1^0} \gtrsim 1$ TeV (right panel, upper edge of the brown-shaded area).

On the other hand, the upper end of the exclusion ranges (17) and (18) is mainly determined by how *long* a decay lifetime an observation can probe, and in this regard, it is the energy injection limits from the *Planck* CMB anisotropy measurements that dominate the current constraints. The *Planck* CMB anistropy limit is most evident in the right panel of Fig. 2 (lower edge of the red-shaded area), and extends to lifetimes well in excess of $\tau \sim 10^{20}$ s, i.e., longer than the lifetime of the Universe thus far ($t \sim 4 \times 10^{17}$ s). Improvement from a future CMB anisotropy measurement by LiteBIRD+CMB-S4 in this region will however likely be marginal (right panel, lower edge of the brown-shaded area), as the reach in decay lifetime of these future observations is unlikely to outperform the *status quo* by more than a factor of a few (see also Fig. 1).

It is also interesting to consider what limits Lyα observations impose on the gravitino superWIMP parameter space; the corresponding exclusion region is shaded pink in both the left and right panels of Fig. 2. At face value the Lyα bounds do not appear to add much to the energy injection constraints already discussed above in either the $(m_{\chi_1^0}, m_{\tilde{G}})$- or $(m_{\chi_1^0}, \epsilon_{em})$-plane. However, while BBN and CMB observations probe the electromagnetic energy injected into the cosmic plasma, Lyα is sensitive to the free-streaming properties of the gravitino itself and therefore offers a somewhat

different perspective on the superWIMP scenario. It also provides a useful constraint on those scenarios not considered in this work wherein the NLSP does not decay electromagnetically (e.g., decay into neutrinos). We devote several paragraphs below to explain the essential features of the Lyα constraint on the gravitino superWIMP parameter space.

Observe first in the left panel of Fig. 2 that Lyα rules out a substantial region around neutralino masses of $\mathcal{O}(1)$ GeV to $\mathcal{O}(1)$ TeV in the $(m_{\chi_1^0}, m_{\tilde{G}})$-plane, and, like the energy injection constraints, provides an upper limit on viable values of $m_{\tilde{G}}$, albeit a much weaker one. This may at first glance appear counter-intuitive to the common understanding that Lyα observations limit the particle masses of free-streaming dark matter from below, to $m_{\rm WDM} \gtrsim \mathcal{O}(1)$ keV. To reconcile these seemingly conflicting results, note first of all that thermal WDM mass constraints in the literature typically carry the assumption that the WDM makes up all of the dark matter content of the Universe. On the other hand, the upper limit on $m_{\tilde{G}}$ in Fig. 2 arises from the fact that once the WDM fraction – defined here as $f_{\rm WDM} = m_{\tilde{G}}/m_{\chi_1^0}$ (see Sect. 3.4) – drops below $f_{\rm WDM} < 0.15$, the free-streaming properties of the gravitino LSP become unconstrainable by current observations (see also Table 1). In fact, this upper limit on $m_{\tilde{G}}$ parallels cosmological bounds on the absolute mass scale of Standard-Model neutrinos, where extremely small masses (and hence very large free-streaming scales) cannot be constrained because the energy density low-mass neutrinos contribute to the total dark matter content is too minute for their free-streaming effects to be observable.

Secondly, free-streaming is a kinematic effect dependent only on the characteristic *velocity* of the WDM in question. Its use as tool to constrain WDM masses to $\mathcal{O}(1)$ keV masses and above rests strongly on the assumption that the WDM has been produced via scattering processes with the SM thermal bath, such that the WDM population inherits the characteristic momentum (or temperature) of the bath *even* in the event that thermalisation is incomplete. In the case of production via NLSP decay, however, the characteristic momentum inherited by the LSP at production, $p_\star = \epsilon_{\rm em} m_{\chi_1^0}$, is unrelated to the properties of the SM thermal bath; rather, it is determined by the NLSP mass – which, in our scenarios, is typically orders of magnitude larger than the SM bath temperature at the time of decay – and the NLSP-LSP mass gap. Consequently, the LSP masses constrained by velocity-based free-streaming arguments also fall in a range of orders of magnitude above naïve expectations.

Turning our attention now to the Lyα limits displayed in the right panel of Fig. 2, we see immediately that there is in fact also a lower limit on viable values of $m_{\tilde{G}}$, manifesting in the $(m_{\chi_1^0}, \epsilon_{\rm em})$-plane as a lower limit on viable values of $\epsilon_{\rm em}$ at $m_{\chi_1^0} \gtrsim 1$ TeV (right edge of the pink-shaded region). To explain this limit, recall that in this plot, the energy injection is generally tiny, i.e., $\epsilon_{\rm em} \ll 0.5$, such that the WDM fraction is saturated at $f_{\rm WDM} = 1$ over the bulk of the displayed parameter region. Thus, the same $f_{\rm WDM} = 1$ free-streaming horizon limit ($\lambda_{\rm FS} \lesssim 0.0708\, h^{-1}$Mpc from Table 1) applies (almost) everywhere. Indeed, the right edge of the Lyα exclusion region aligns closely with the contours of constant free-streaming horizon $\lambda_{\rm FS}$ in the right panel of Fig. 2 as expected. In contrast, the same edge in the $(m_{\chi_1^0}, m_{\tilde{G}})$-plane in the left panel shows no such alignment; rather, the edge shifts to higher values of $\lambda_{\rm FS}$ as we decrease $m_{\tilde{G}}$, reflecting the weakening of the Lyα limit on $\lambda_{\rm FS}$ with decreasing $f_{\rm WDM}$ evident in Table 1. [15]

Finally, we remark that collider experiments constrain only a very tiny region of the gravitino superWIMP parameter space, in a spot where an extremely large hierarchy exists between $m_{\chi_1^0}$ and $m_{\tilde{G}}$ so as to produce a detectable LLP signal (left panel of Fig. 2, purple-shaded region). Specifically, reinterpreting the ATLAS and CMS limits from Refs. [84,85], which are presented on the $(m_{\chi_1^0}, \tau)$-plane with GMSB SPS8 benchmarks as the reference model, we find that for neutralino masses up to $m_{\chi_1^0} \simeq 400$ GeV, current LHC data exclude gravitino masses up to $m_{\tilde{G}} \simeq 10^{-5}$ GeV. As discussed in Sect. 3.5, LLP search limits are model-dependent: thus the LHC exclusion region presented in Fig. 2 can move (within small confines) depending on the model specifics of the search analysis.

Note also that our LHC exclusion region has a vertical cut-off at $m_{\chi_1^0} \simeq 200$ GeV; this follows simply from the fact that Refs. [84,85] had chosen to focus on a specific region of parameter space in their analyses. It is not inconceivable that current LHC data could constrain also some parts of the parameter region to the left of the cut-off; it is however extremely unlikely that the exclusion region extends all the way to $m_{\chi_1^0} = 0$, as the search would become background-limited.

For completeness we estimate also the sensitivity of the high-luminosity LHC (HL-LHC) run, by simply rescaling the current LHC constraint to 3000 fb^{-1} integrated luminosity (left panel, blue-shaded region). We find that HL-LHC can improve the reach in gravitino masses by at most an order of magnitude to $m_{\tilde{G}} \simeq 10^{-4}$ GeV for neutralino masses up to

[15] References [75,76] have also derived Lyα constraints on particle decay scenarios. It is however difficult to make quantitative comparisons of our results with these previous works, because of the different assumptions involved. One major difference, for example, is that we always assume the NLSP to be produced in the correct abundance (or at some fixed abundance as explored in Appendices B and C), while [75,76] demand that the decay product makes up the entire observed dark matter abundance irrespective of the original NLSP abundance, i.e., they "marginalise" over the NLSP abundance. As demonstrated in Appendix C, qualitatively, over-producing NLSP tends to shift (but not extend) the Lyα sensitivity region to smaller LSP masses. This understanding may explain why these earlier analyses find lower limits on the LSP mass in the keV region.

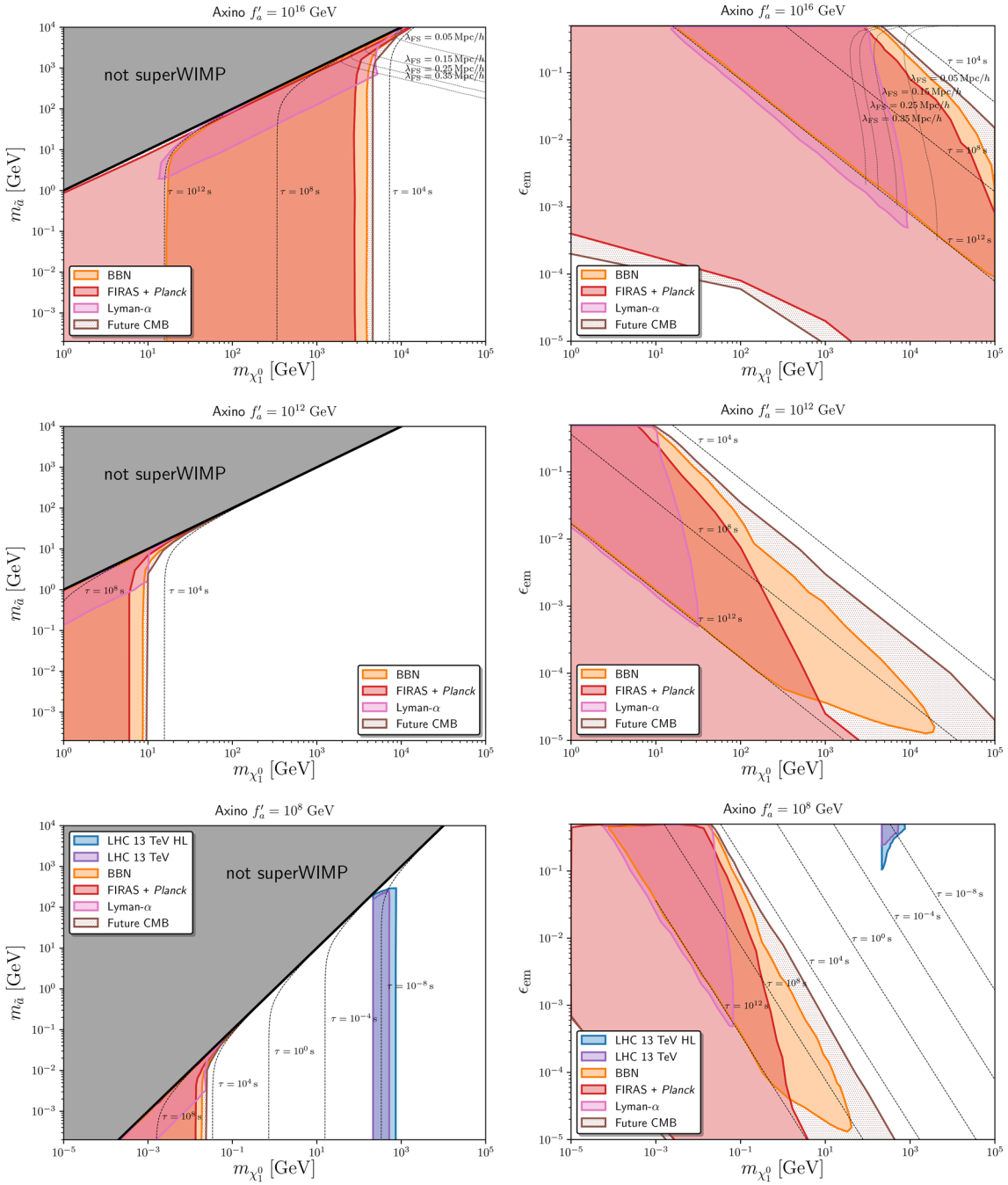

Fig. 3 Same as Fig. 2, but for the axino superWIMP assuming three different values of the axion decay constant. We have however omitted plotting the lines of constant $\lambda_{\rm FS}$ in the cases of $f'_a = 10^{12}$, 10^8 GeV, as well as the exclusion region at $m_{\chi_1^0} \lesssim 34$ GeV, which we in any case do not enforce

$m_{\chi_1^0} \simeq 1$ TeV. We note however that the projection to HL-LHC originating from LLP searches depend on whether the neutralino is produced with enough cross-section and is not ruled out by jets + missing energy searches.

4.2 Axino

Analogously to Figs. 2, 3 shows the current and projected cosmological and collider constraints on the axino super-

WIMP parameter space in the $(m_{\chi_1^0}, m_{\tilde{a}})$-plane (left panels) and the $(m_{\chi_1^0}, \epsilon_{\rm em})$-plane (right panels), assuming three different values of the axion decay constant $f_a' \equiv f_a/N \in [10^8, 10^{12}, 10^{16}]$ GeV. As in Fig. 2, overclosure excludes in principle $m_{\chi_1^0} \lesssim 34$ GeV if the neutralino is produced via thermal freeze-out; we have however omitted plotting this constraint in Fig. 3 since it can be easily circumvented by other production mechanisms and we in any case do not enforce it.

As can be gleaned from the neutralino-to-axino decay width (7), with $\epsilon_{\rm em}$ held fixed, the decay lifetime scales as $\tau \propto f_a'^2/m_{\chi_1^0}^3$. Thus, in both the $(m_{\chi_1^0}, m_{\tilde{a}})$- and $(m_{\chi_1^0}, \epsilon_{\rm em})$ planes, we generally expect experimental constraints (cosmological and collider) to apply to larger neutralino mass values as we crank up f_a'. Indeed, as is evident in the left panels of Fig. 3, the right edges of the cosmological exclusion regions (BBN, FIRAS+*Planck*, and FutureCMB) mostly align with the lifetime reach of the observations at the short end. Where the neutralino and axino masses are strongly hierarchical (so that $\epsilon_{\rm em} \simeq 0.5$), the decay lifetime also becomes independent of $m_{\tilde{a}}$. Consequently, the points at which the edges of the exclusion regions intersect the horizontal $m_{\chi_1^0}$-axis also scale as $f_a'^{2/3}$. As in the case of the gravitino superWIMP, the most stringent limit at the short end of τ comes currently from observations of the light element abundances (shaded orange), although there is also a small region in which BBN constraints are outperformed by Lyα observations (shaded pink).

Interestingly, for a large range of neutralino masses subject to cosmological energy injection constraints – specifically, where the aforementioned scaling of the $m_{\chi_1^0}$ bound applies – the same constraints also rule out a massless axino ($m_{\tilde{a}} = 0$). It is only in the degenerate ($m_{\chi_1^0} \simeq m_{\tilde{a}}$ and $\epsilon_{\rm em} \ll 0.5$) region where the excluded parameter space does not necessarily include $m_{\tilde{a}} = 0$. This conclusion is independent of the assumed value of f_a' and stands in stark contrast to the gravitino superWIMP case, where the lower end of the exclusion region is always finite in $m_{\tilde{G}}$, whose precise value depends on our choice of $m_{\chi_1^0}$ (see Eqs. (17) and (18)). Cosmological energy injection constraints therefore appear to have more drastic consequences for the axino than for the gravitino.

At the long end of the decay lifetime ($\tau \sim 10^{12} - 10^{23}$ s), the constraints again originate primarily from the *Planck* measurements of the CMB anisotropies (although we remind the reader here that the BBN limits have been cut off in this region only because of the lack of available calculations in the literature, while for the Lyα constraints our estimates of the free-streaming horizon may not suffice to model the observable effects of this parameter region; see Sects. 3.1 and 3.4 for details). The limits imposed by the CMB anisotropies at this end are most easily discernible in the right panels of Fig. 3 showing the $(m_{\chi_1^0}, \epsilon_{\rm em})$-plane (lower edge of red-shaded area), and translate generally into an upper limit on the axino mass. Taking all observations into account, for the three values of f_a' considered in this work and various fixed neutralino mass values, we find that cosmology constrains the axino mass $m_{\tilde{a}}$ to lie within the following ranges:

- $f_a' = 10^{16}$ GeV:

$$\begin{aligned} m_{\chi_1^0} &= 100\ \text{GeV} &&: 0 \lesssim m_{\tilde{a}}/\text{GeV} \lesssim 99.992, \\ m_{\chi_1^0} &= 1\ \text{TeV} &&: 0 \lesssim m_{\tilde{a}}/\text{GeV} \lesssim 999.98, \\ m_{\chi_1^0} &= 2.7\ \text{TeV} &&: 0 \lesssim m_{\tilde{a}}/\text{GeV} \lesssim 2699.990, \\ m_{\chi_1^0} &= 4\ \text{TeV} &&: 530 \lesssim m_{\tilde{a}}/\text{GeV} \lesssim 3999.986, \end{aligned} \tag{19}$$

- $f_a' = 10^{12}$ GeV:

$$\begin{aligned} m_{\chi_1^0} &= 100\ \text{GeV} &&: 98 \lesssim m_{\tilde{a}}/\text{GeV} \lesssim 100 - 5 \times 10^{-5}, \\ m_{\chi_1^0} &= 1\ \text{TeV} &&: 998.9 \lesssim m_{\tilde{a}}/\text{GeV} \lesssim 1000 - 8 \times 10^{-5} \end{aligned} \tag{20}$$

- $f_a' = 10^{8}$ GeV:

$$m_{\chi_1^0} = 10\ \text{GeV} \quad : 0.00017 \lesssim m_{\tilde{a}}/\text{GeV} \lesssim 0.000019. \tag{21}$$

Thus, in terms of ruling out a large chunk of interesting particle masses in the GeV-to-TeV region conventionally of interest to collider searches, cosmological constraints have the strongest impact for large axion decay constants in the vicinity of $f_a' = 10^{16}$ GeV, ruling out neutralino masses of up to ~ 3 TeV and all possible axino masses up to the degenerate limit. The equivalent constraints in the same mass region are currently significantly weaker for smaller f_a' values (i.e., $f_a' = 10^{12}, 10^8$).

Having said the above however, we also observe that only for $f_a' \lesssim 10^8$ GeV does the neutralino lifetime become short enough to be sensitive to LLP searches at the LHC (bottom left panel of Fig. 3, purple- and blue-shaded areas). Specifically, for $f_a' = 10^8$ GeV, LLP searches at the LHC currently rule out neutralino and axino masses in the $\sim$ 50–500 GeV region, which can be extended to $\sim$ 80–800 GeV in the future by HL-LHC. As in the gravitino case, reinterpretation of published ATLAS and CMS limits from the model-specific analyses of [84,85] (see Sect. 4.1) forces us to impose a cut-off on the LHC exclusion regions, this time at $m_{\tilde{a}} \sim 100$ GeV, which may or may not be indicative of the true sensitivity of the LHC searches. Nonetheless, as can be seen in Fig. 3, cosmological observations clearly have no sensitivity to the parameter combinations probed at colliders. The complementarity between cosmological observations and collider searches is therefore self-evident.

5 Conclusions

We have revisited in this work cosmological constraints on Supersymmetric superWIMPs, and demonstrated that cosmology provides strong limits on two of the most well motivated candidates, the gravitino and the axino.

For the gravitino, the totality of cosmological constraints from energy injection and free-streaming considerations exclude neutralino and gravitino masses from a few eV to several TeV (Fig. 2), effectively ruling out a large part of the gravitino superWIMP parameter space. Measurements of the CMB anisotropies by the *Planck* CMB mission in particular extend the lifetime reach of cosmological observations to unprecedentedly long time scales (up to lifetimes of $\tau \simeq 10^{23}$ s, several orders of magnitude longer than the lifetime of the Universe thus far). This enables us to close a large gap in the gravitino mass in the degenerate region ($m_{\tilde{G}} \simeq m_{\chi_1^0}$) previously allowed by observations of the light element abundances and CMB spectral distortions by COBE/FIRAS. Future CMB probes such has CMB-S4 and LiteBird will contribute to expanding this excluded region. The case where the neutralino is overabundant by a significant amount is not captured in this analysis, which requires a dedicated work to capture the corresponding impact on early-universe cosmology.

In contrast, LLP searches at the LHC have a significantly smaller scope in terms of size of the gravitino superWIMP parameter space accessible to these searches, and the improvement expected from the upcoming HL-LHC is modest in comparison with the already vast parameter region covered by cosmological observations – up to masses of $\mathcal{O}(100)$ TeV, well beyond the kinematic reach of current and future collider experiments. Collider bounds are furthermore model-dependent and hinge on the neutralino production mechanism from cascade decay assumed in the analysis. In contrast, cosmological constraints are conditioned only on the premise that a population of neutralino NLSPs is produced in some reasonable abundance in the early Universe and that this population decays electromagnetically. Both assumptions can be easily satisfied independently of the model specifics. Notwithstanding their versatility, we emphasise that cosmological and collider bounds occupy completely different regions of the gravitino superWIMP parameter space, and certain parts of this parameter space remain as yet inaccessible to either. Thus, both types of probes remain as relevant as ever in the quest for BSM physics.

Similar conclusions hold for the axino superWIMP assuming $f_a' = 10^{16}$ GeV, where again a large range of neutralino and axino masses up to the TeV scale are excluded, including $m_{\tilde{a}} = 0$ (Fig. 3). For lower values of the axino decay constant f_a', the excluded region shifts to lower neutralino masses approximately as $f_a'^{2/3}$, such that for $f_a' \lesssim 10^{12}$ GeV the neutralino and axino masses excluded by cosmology typically fall below $\sim$ 10 GeV. We note however that collider constraints do not exist for $f_a' \gtrsim 10^9$ GeV, as the neutralino decay width is suppressed by $f_a'^{-2}$ and substantial decay occurring within the detector volume is simply too improbable for large f_a' values. Thus, while some parts of the axino superWIMP parameter space indeed lie within the reach of the LHC, our analysis here shows that within this class of models, the most model-independent and sweeping constraints in fact originate from cosmology.

Lastly, while this work concerns SUSY superWIMPs, we note that the same cosmological constraints apply also to a large variety of well-motivated BSM scenarios that predict extremely weakly-coupled particles (either from symmetries or by the nature of the interactions) with limited signatures in conventional high-energy collider experiments. These include models of cosmological relaxation [94], clockwork [95,96], long-lived KK gravitons and radions [97], and continuum dark matter [98], etc. The largely model-independent analysis presented in this work can be easily adapted to investigate how precision cosmological observations impact on such BSM scenarios. We leave these studies for future works.

Acknowledgements We thank Geneviève Bélanger, Daniel R. Green, Paul D. Jackson, and Matteo Lucca for useful discussions. Support for this work has been provided by the University of Adelaide and the Australian Research Council through the Centre of Excellence for Dark Matter Particle Physics (CE200100008). DS is partially supported through the the University of New South Wales, startup grant PS-71474. Y^{3}W is supported in part by the Australian Government through the Australian Research Council's Future Fellowship (FT180100031) and Discovery Project (DP240103130).

Data Availability Statement This manuscript has no associated data or the data will not be deposited. [Authors' comment: All data generated during this study are contained in this published article.]

Code Availability Statement My manuscript has no associated code/software. [Authors' comment: The code/software generated during and/or analysed during the current study is available from the corresponding author on reasonable request.]

Funded by SCOAP^3.

Appendix A: The LSP momentum distribution

Consider the decay process $\chi_1^0 \to \text{LSP} + \gamma$, whose rate in the rest frame of χ_1^0 (which coincides with the cosmic frame) is Γ. The comoving number density of χ_1^0 is

$$n_{\chi_1^0}(t) = \frac{\Omega_{\rm DM}\rho_{\rm crit}}{m_{\chi_1^0}} \exp\left(-\Gamma t\right), \tag{A1}$$

where $\rho_{\rm crit}$ is the present-day critical density, and we have assumed χ_1^0 to be produced at an abundance that would match the observed reduced dark matter density $\Omega_{\rm DM}$ in the absence of decay. Demanding that the rate of change of the comoving LSP number density $n_{\rm LSP}$ matches the negative rate of change of $n_{\chi_1^0}$, the evolution equation for $n_{\rm LSP}$ can be written as

$$\frac{{\rm d}n_{\rm LSP}}{{\rm d}t} = \Gamma n_{\chi_1^0} = \frac{\Omega_{\rm DM}\rho_{\rm crit}}{m_{\chi_1^0}} \Gamma \exp\left(-\Gamma t\right), \tag{A2}$$

or equivalently in terms of the scale factor R,

$$\frac{{\rm d}n_{\rm LSP}}{{\rm d}\ln R} = \frac{\Omega_{\rm DM}\rho_{\rm crit}}{m_{\chi_1^0}} \left(\frac{R}{R_\Gamma}\right)^n n \exp\left[-\left(\frac{R}{R_\Gamma}\right)^n\right], \tag{A3}$$

where $n = 2, 3/2$ applies to radiation domination and matter domination respectively, and R_Γ is the scale factor at the time $t = 1/\Gamma$.

Observe that, at the moment of production, the LSP always carries a physical momentum $p_\star = \epsilon_{\rm em} m_{\chi_1^0}$, irrespective of the the time of of production. Universal expansion, however, will cause the momentum to redshift, such that an LSP produced at a scale factor R will be observed today uniquely with a physical momentum of $p = p_\star R$. Thus, in the same way that we use R as a proxy for time, we can also use the observed momentum p as a proxy for R, and recast Eq. (A3) as

$$\frac{{\rm d}n_{\rm LSP}}{{\rm d}\ln p} = \frac{\Omega_{\rm DM}\rho_{\rm crit}}{m_{\chi_1^0}} \left(\frac{p}{p_\star R_\Gamma}\right)^n n \exp\left[-\left(\frac{p}{p_\star R_\Gamma}\right)^n\right]. \tag{A4}$$

Approximating the transition from radiation to matter domination to be instantaneous at $R_{\rm eq}$, LSP produced during radiation domination ($n = 2$) can be observed today with a physical momentum up to $p_\star R_{\rm eq}$, while those arising from decay during matter domination ($n = 3/2$) will have momenta in the range $p_\star R_{\rm eq} < p \leq p_\star$. Integrating Eq. (A4) under this approximation and assuming no pre-existing LSP population then yields Eq. (10).

Appendix B: Constraints on the superWIMP parameter space for under-production of neutralinos

Figures 4 and 5 show constraints in the $(m_{\chi_1^0}, m_{\rm LSP})$- and $(m_{\chi_1^0}, \epsilon_{\rm em})$-planes for a gravitino LSP and an $f_a = 10^{16}$ GeV axino LSP, respectively, assuming that the neutralino population is produced at only the 10% and 0.1% of the abundance required to match the observed DM energy density.

Relative to the case in which the neutralino abundance matches the observed DM abundance, under-production cases generally result in a shrinkage in the parameter regions constrained by BBN and CMB energy injection bounds. This shrinkage is primarily due to a reduced sensitivity to (i) the short lifetimes ($\tau \lesssim 10^4$ s) on the $(m_{\chi_1^0}, m_{\rm LSP})$-plane, and (ii) the energy injection fraction for extremely long lifetimes ($\tau \gg 10^{12}$ s). Observe also that the Lyα constraints have completely disappeared from Figs. 4 and 5. This is because an under-production of neutralinos also implies an under-production of gravitino and axino warm dark matter. At, e.g., 10% under-production of χ_1^0, the WDM fraction is at most $f_{\rm WDM} = 0.1$, which falls below the smallest constrainable WDM fraction by the Lyα data of Table 1.

Appendix C: Constraints on the superWIMP parameter space for over-production of neutralinos

It is also interesting to see how the cosmologically-constrained regions change when the neutralino population is *over*-produced. Figures 6 and 7 show the corresponding constraints in the $(m_{\chi_1^0}, m_{\rm LSP})$-plane for a gravitino LSP and an $f_a = 10^{16}$ GeV axino LSP, respectively, assuming the neutralino population to be over-produced by a factor of 10 relative to the observed DM abundance.

Over-production scenarios are subject to two additional constraints: (i) the maximum mass of the LSP is always limited by $m_{\rm LSP}/m_{\chi_1^0} \leq 1/F_{\rm over}$, where $F_{\rm over}$ is the over-production factor (10 in the case of Figs. 6 and 7), and (ii) the NLSP-to-LSP decay must occur at a sufficiently early time such that no substantial DM and radiation excesses remain at CMB times to interfere with the standard expansion history. Condition (i) is straightforward to apply and immediately rules out the light grey region in Figs. 6 and 7. Furthermore, for an over-production factor of 10, the viable parameter regions under condition (i) – i.e., $m_{\rm LSP}/m_{\chi_1^0} \lesssim 1/10$ – must yield an energy injection fraction no less than $\epsilon_{\rm em} \simeq 0.5$ irrespective of $m_{\chi_1^0}$. In other words, the entire $(m_{\chi_1^0}, \epsilon_{\rm em})$-plane up to $\epsilon_{\rm em} \simeq 0.5$ is excluded; for this reason we have chosen not to plot it.

Condition (ii) can be implemented as two separate constraints, one on the DM abundance and one on the radiation energy. For the former, we demand that combined neutralino and LSP abundance, given as a function of time by

$$\Omega_{\rm LSP} + \Omega_{\chi_1^0} = F_{\rm over}\Omega_{\rm DM}\left\{\frac{m_{\rm LSP}}{m_{\chi_1^0}} + \left[1 - \frac{m_{\rm LSP}}{m_{\chi_1^0}}\right]\exp(-\Gamma t)\right\}, \tag{C1}$$

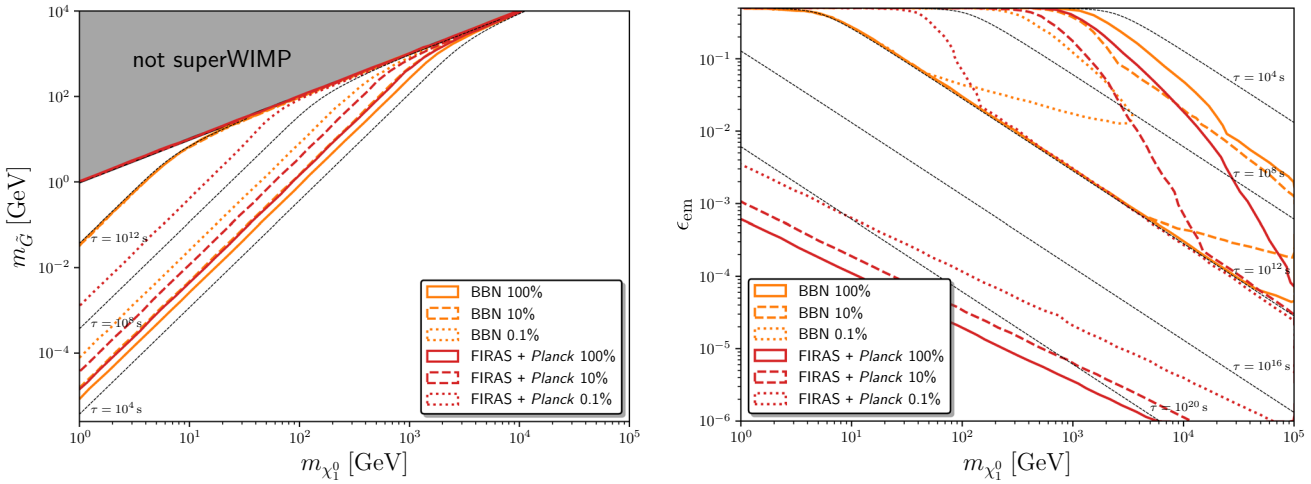

Fig. 4 Constraints on the gravitino superWIMP parameter space from BBN and current CMB data for a neutralino population produced at an energy density corresponding to 100% (solid lines), 10% (dahed lines) and 0.1 % (dotted lines) of the observed DM energy density

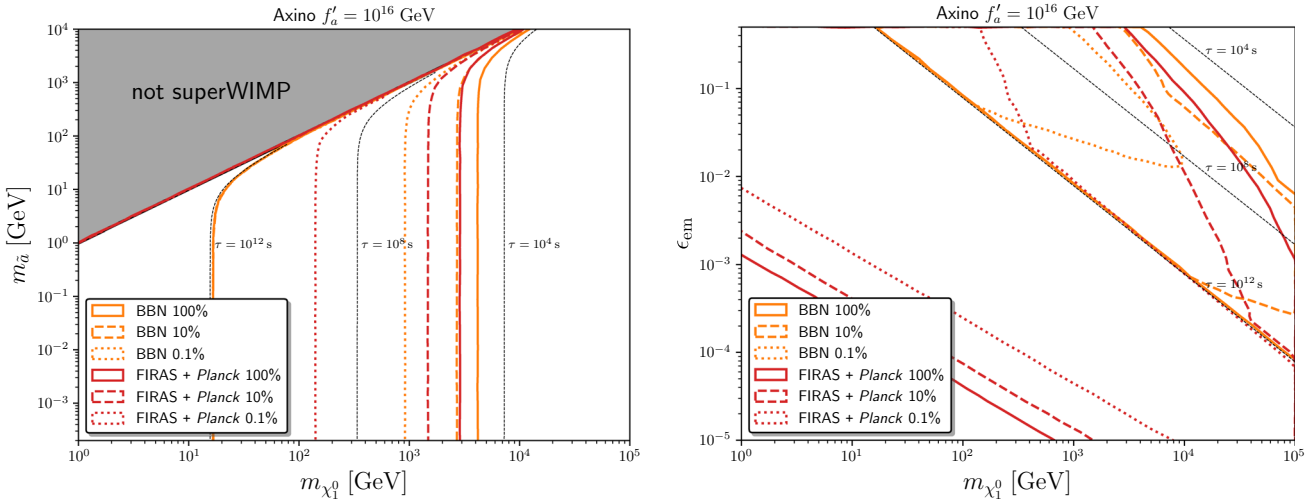

Fig. 5 Same as Fig. 4, but for an axino LSP with $f_a = 10^{16}$ GeV

not to exceed the observed DM abundance by more than a few percent at $z \lesssim 10^4$. That is, we demand that the DM abundance should already be more or less "correct" by the time the smallest scales probed by the CMB anisotropies enter the horizon, so as not create too much deviation in the evolution history of the anisotropies from the standard case. Since Eq. (C1) is a decreasing function of time, it suffices to demand approximate concordance at $z = 10^4$, i.e., the time point at which the impact of (C1) on the CMB anisotropies is the largest, and we impose a maximum deviation of 10%, motivated by a conservative 95% C.L. error on the observed DM abundance.[16] Then, the condition becomes a simple upper limit on the neutralino lifetime,

$$\tau \lesssim \frac{2 \times 10^{11}\ \text{s}}{\ln\left[\dfrac{m_{\chi_1^0} - m_{\rm LSP}}{((1+x)/F_{\rm over})m_{\chi_1^0} - m_{\rm LSP}}\right]}, \tag{C2}$$

where the prefactor 2×10^{11} s corresponds to the age of the universe at $z = 10^4$, and $x = 0.1$ for a 10% tolerance. For masses saturating $m_{\rm LSP}/m_{\chi_1^0} = 1/F_{\rm over} = 1/10$, Eq. (C2) is

[16] While it is commonly said that CMB anisotropy measurements constrain the dark matter density $\Omega_{\rm DM}h^2$ to 2%-level uncertainty at 95% [38], this statement is in fact strongly dependent on the background cosmology and free parameters adopted in the parameter estimation analysis. Analyses that allow for a non-standard radiation content (i.e., $N_{\rm eff} \neq 3.044$) and/or non-zero neutrino masses in particular typically yield significantly larger (up to a factor of four) error bars for $\Omega_{\rm DM}h^2$ because of these parameters' degeneracy with $\Omega_{\rm DM}h^2$. See the Planck Legacy Archive (https://pla.esac.esa.int/) for a thorough exploration of how cosmological constraints vary with respect to model assumptions and/or data used.

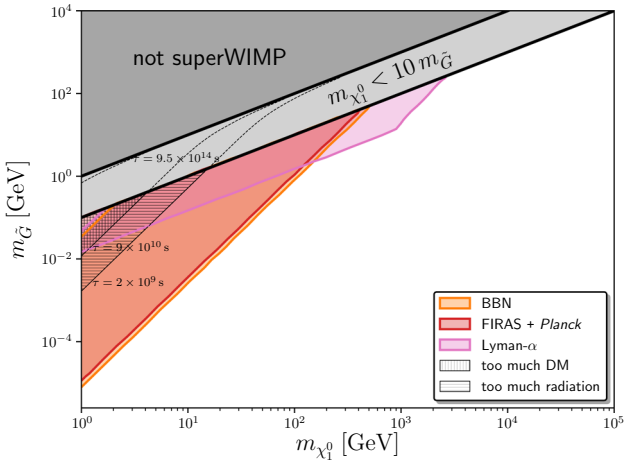

Fig. 6 Constraints on the gravitino superWIMP parameter space from BBN and current CMB data for a neutralino population produced at an energy density ten times above the observed DM energy abundance. Relative to scenarios in which the neutralino population matches or is under the observed DM abundance (Figs. 2 and 4), over-production scenarios are subject to additional constraints on excess DM energy density (vertical hatch) and excess radiation energy density (horizontal hatch). The light grey region corresponds to $m_{\rm LSP}/m_{\chi_1^0} > 1/f_{\rm over}$, where $f_{\rm over} = 10$ is the over-production factor, and is by definition incompatible

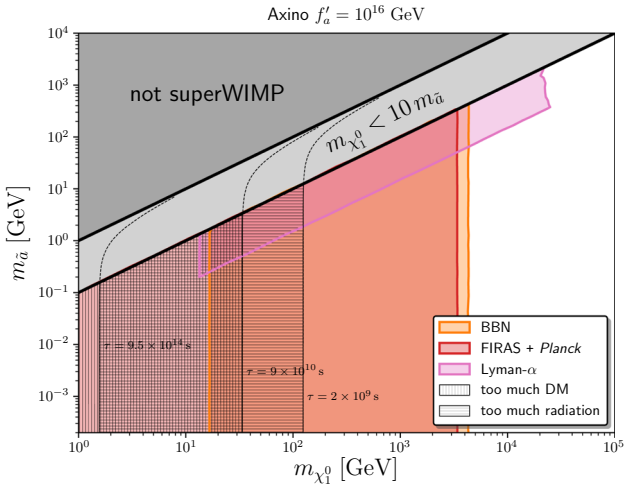

Fig. 7 Same as Fig. 6, but for an axino LSP with $f_a = 10^{16}$ GeV

equivalent to a constraint of $\tau \lesssim 4 \times 10^{10}$ s on the neutralino lifetime. For mass combinations not saturating the $1/F_{\rm over}$ bound, the constraint on τ will be weaker, but not significantly so: indeed, in the limit $m_{\rm LSP}/m_{\chi_1^0} \to 0$, the upper limit on the neutralino lifetime asymptotes to $\tau \lesssim 9 \times 10^{10}$ s. The vertically-hatched regions in Figs. 6 and 7 are excluded by this lifetime constraint consideration. Note that while we have imposed a tolerance $x = 0.1$ on the DM abundance (C1), in practice the form of the neutralino lifetime constraint (C2) implies an extremely weak dependence of the excluded superWIMP parameter region on the choice of x, provided $x \ll 1$.

To implement the constraint on the excess radiation density in the CMB window, we note first of all that the time evolution of the excess radiation density from NLSP-to-LSP decay is described by

$$\frac{{\rm d}\rho_{\rm em}}{{\rm d}t} + 4H(t)\rho_{\rm em} = m_{\chi_1^0}\epsilon_{\rm em} R^{-3} \frac{{\rm d}n_{\rm LSP}}{{\rm d}t} = F_{\rm over}\Omega_{\rm DM}\rho_{\rm crit}\epsilon_{\rm em} R^{-3}\Gamma \exp(-\Gamma t). \tag{C3}$$

Defining the comoving radiation energy density to be $\tilde{\rho}_{\rm em} \equiv \rho_{\rm em} R^4$ and adopting the scale factor R in place of the time variable t, Eq. (C3) can be recast into

$$\frac{{\rm d}\tilde{\rho}_{\rm em}}{{\rm d}R} = F_{\rm over}\Omega_{\rm DM}\rho_{\rm crit}\epsilon_{\rm em} \left(\frac{R}{R_\Gamma}\right)^n n \exp\left[-\left(\frac{R}{R_\Gamma}\right)^n\right], \tag{C4}$$

where $n = 2, 3/2$ during radiation domination and matter domination, respectively. Evaluating Eq. (C4) for $n = 2$ from 0 to $R_{\rm eq}$ and then for $n = 3/2$ from $R_{\rm eq}$ to $R > R_{\rm eq}$, we find the solution

$$\tilde{\rho}_{\rm em} = F_{\rm over}\Omega_{\rm DM}\rho_{\rm crit}\epsilon_{\rm em} \times \left\{ \frac{1}{2} R_\Gamma \sqrt{\pi}\, {\rm erf}\left(\frac{R_{\rm eq}}{R_\Gamma}\right) - R_{\rm eq} \exp\left[-\left(\frac{R_{\rm eq}}{R_\Gamma}\right)^2\right] + R' \left(\frac{R'}{R_\Gamma}\right)^{3/2} E_{-2/3}\left[\left(\frac{R'}{R_\Gamma}\right)^{3/2}\right]\Bigg|_{R'=R}^{R'=R_{\rm eq}} \right\}, \tag{C5}$$

where erf stands for the error function, and $E_n(z) \equiv \int_1^\infty {\rm d}t\, e^{-zt}/t^n$ is the exponential integral function.

Assuming three SM neutrinos of fixed energy densities, the energy density in electromagnetic radiation during the CMB epoch is measured to a 95% uncertainty of $\sim 10\%$, motivated by the current $\sim 10\%$ uncertainty on the effective number of neutrinos $N_{\rm eff} \equiv (1/0.227)(\rho_\nu/\rho_{\rm em})$, depending on exactly how the parameter estimation analysis is done (see Footnote 16). Then, a simple constraint can be set on R_Γ by demanding that $\tilde{\rho}_{\rm em}/\rho_{\rm crit}$ conform within errors to the measured value in the CMB window $z \simeq z_\star \to 10^4$, where $z_\star \simeq 1100$ is the redshift of recombination. Since $\tilde{\rho}_{\rm em}$ increases with time, we choose to impose a 10% tolerance on the excess radiation at $z = z_\star$, where the impact of $\tilde{\rho}_{\rm em}$ on the CMB primary anisotropies is the largest. Then, solving Eq. (C5) for $F_{\rm over} = 10$, $\epsilon_{\rm em} = 0.5$, and $\Omega_{\rm DM} = 0.244$ [38], and applying the $\Omega_{\rm rad}$ constraint, we find that

$$R_\Gamma \simeq 9 \times 10^{-6} \to 1.5 \times 10^{-2}, \tag{C6}$$

or, equivalently,

$$\tau \simeq 2 \times 10^9 \to 9.5 \times 10^{14}\ \text{s}, \tag{C7}$$

can be excluded irrespective of the particle masses. This exclusion region is indicated with horizontal hatching in Figs. 6 and 7. Reducing the tolerance from 10% to, e.g., 5% has but a minor impact on the exclusion region: the boundaries shift by less than a factor of two, practically indiscernible on a log-log plot spanning five to ten orders of magnitude in each direction.

Note that this excess radiation energy constraint applies in principle also to scenarios in which the NLSP is produced at the correct abundance or is under-produced. However, these constraint are uncompetitive: for NLSP produced at the correct abundance, i.e., $F_{\text{over}} = 1$, the exclusion region corresponds to

$$R_\Gamma \simeq 9 \times 10^{-5} \to 3 \times 10^{-3}, \tag{C8}$$

or equivalently,

$$\tau \simeq 2 \times 10^{11} \to 8 \times 10^{13}\ \text{s}, \tag{C9}$$

i.e., a mere sliver of the parameter superWIMP space already excluded by CMB and BBN energy injection bounds depicted in Figs. 2 and 3; in cases of underproduction, e.g., $F_{\text{over}} \leq 1/10$ in Figs. 4 and 5, equivalent constraints do not even exist.

Other than the above new conditions, the constraints on the $(m_{\chi_1^0}, m_{\text{LSP}})$-plane from BBN and CMB energy injection considerations are only marginally tighter than those we saw earlier in Figs. 2 and 3, where the neutralino had been assumed to be produced at the correct abundance. On the other hand, the Lyman-α exclusion regions, while looking generally similar in shape as before, have "shifted downwards" by a factor of 10 (corresponding to the overproduction factor). In the case of the axino, the exclusion region also protrudes further to the right following the free-streaming horizon λ_{FS} contours (see Fig. 3), allowing Lyα to outperform the energy injection constraints by a larger margin than in Figs. 2 and 3. Importantly, however, the Lyα exclusion regions remain bounded from below by $f_{\text{WDM}} = 0.15$, or, equivalently in this case, by $m_{\text{LSP}}/m_{\chi_1^0} = 0.15/F_{\text{over}}$, since once the LSP mass drops too low to make up a substantial fraction of the DM, its free-streaming effects also become unobservable.

References

1. **ATLAS** Collaboration, G. Aad et al., Search for pair production of squarks or gluinos decaying via sleptons or weak bosons in final states with two same-sign or three leptons with the ATLAS detector. arXiv:2307.01094 [hep-ex]
2. **ATLAS** Collaboration, G. Aad et al., Search for direct production of winos and higgsinos in events with two same-charge leptons or three leptons in pp collision data at $\sqrt{s} = 13$ TeV with the ATLAS detector. arXiv:2305.09322 [hep-ex]
3. **CMS** Collaboration, Search for stealth SUSY in final states with two photons, jets, and low missing transverse momentum. tech. rep., CERN, Geneva (2023). https://cds.cern.ch/record/2852182
4. **ATLAS** Collaboration, G. Aad et al., Search in diphoton and dielectron final states for displaced production of Higgs or Z bosons with the ATLAS detector in $\sqrt{s} = 13$ TeV pp collisions. arXiv:2304.12885 [hep-ex]
5. **ATLAS** Collaboration, G. Aad et al., Search for long-lived, massive particles in events with displaced vertices and multiple jets in pp collisions at $\sqrt{s}$ = 13 TeV with the ATLAS detector. JHEP**2306**, 200 (2023). https://doi.org/10.1007/JHEP06(2023)200. arXiv:2301.13866 [hep-ex]
6. J.L. Feng, A. Rajaraman, F. Takayama, SuperWIMP dark matter signals from the early universe. Phys. Rev. D **68**, 063504 (2003). https://doi.org/10.1103/PhysRevD.68.063504. arXiv:hep-ph/0306024
7. J.L. Feng, S. Su, F. Takayama, Supergravity with a gravitino LSP. Phys. Rev. D **70**, 075019 (2004). https://doi.org/10.1103/PhysRevD.70.075019. arXiv:hep-ph/0404231
8. J. Abdallah et al., Simplified models for dark matter searches at the LHC. Phys. Dark Univ. **9–10**, 8–23 (2015). https://doi.org/10.1016/j.dark.2015.08.001. arXiv:1506.03116 [hep-ph]
9. J. Bramante, N. Desai, P. Fox, A. Martin, B. Ostdiek, T. Plehn, Towards the final word on neutralino dark matter. Phys. Rev. D **93**(6), 063525 (2016). https://doi.org/10.1103/PhysRevD.93.063525. arXiv:1510.03460 [hep-ph]
10. L. Covi, H.-B. Kim, J.E. Kim, L. Roszkowski, Axinos as dark matter. JHEP **05**, 033 (2001). https://doi.org/10.1088/1126-6708/2001/05/033. arXiv:hep-ph/0101009
11. L. Covi, L. Roszkowski, R. Ruiz de Austri, M. Small, Axino dark matter and the CMSSM. JHEP **06**, 003 (2004). https://doi.org/10.1088/1126-6708/2004/06/003. arXiv:hep-ph/0402240
12. L. Covi, J. Hasenkamp, S. Pokorski, J. Roberts, Gravitino dark matter and general neutralino NLSP. JHEP **11**, 003 (2009). https://doi.org/10.1088/1126-6708/2009/11/003. arXiv:0908.3399 [hep-ph]
13. V.S. Rychkov, A. Strumia, Thermal production of gravitinos. Phys. Rev. D **75**, 075011 (2007). https://doi.org/10.1103/PhysRevD.75.075011. arXiv:hep-ph/0701104
14. R.K. Barman, G. Belanger, B. Bhattacherjee, R. Godbole, G. Mendiratta, D. Sengupta, Invisible decay of the Higgs boson in the context of a thermal and nonthermal relic in MSSM. Phys. Rev. D **95**(9), 095018 (2017). https://doi.org/10.1103/PhysRevD.95.095018. arXiv:1703.03838 [hep-ph]
15. L. Roszkowski, E.M. Sessolo, S. Trojanowski, WIMP dark matter candidates and searches—current status and future prospects. Rep. Prog. Phys. **81**(6), 066201 (2018). https://doi.org/10.1088/1361-6633/aab913. arXiv:1707.06277 [hep-ph]
16. J.L. Feng, A. Rajaraman, F. Takayama, Superweakly interacting massive particles. Phys. Rev. Lett. **91**, 011302 (2003). https://doi.org/10.1103/PhysRevLett.91.011302. arXiv:hep-ph/0302215
17. J.L. Feng, Dark matter candidates from particle physics and methods of detection. Ann. Rev. Astron. Astrophys. **48**, 495–545 (2010). https://doi.org/10.1146/annurev-astro-082708-101659. arXiv:1003.0904 [astro-ph.CO]
18. J.L. Feng, M. Kamionkowski, S.K. Lee, Light gravitinos at colliders and implications for cosmology. Phys. Rev. D **82**, 015012 (2010). https://doi.org/10.1103/PhysRevD.82.015012. arXiv:1004.4213 [hep-ph]
19. A. Arbey, M. Battaglia, L. Covi, J. Hasenkamp, F. Mahmoudi, LHC constraints on gravitino dark matter. Phys. Rev. D **92**(11), 115008 (2015). https://doi.org/10.1103/PhysRevD.92.115008. arXiv:1505.04595 [hep-ph]

20. J.S. Kim, S. Pokorski, K. Rolbiecki, K. Sakurai, Gravitino vs neutralino LSP at the LHC. JHEP **09**, 082 (2019). https://doi.org/10.1007/JHEP09(2019)082. arXiv:1905.05648 [hep-ph]
21. J. Heisig, Gravitino LSP and leptogenesis after the first LHC results. JCAP **04**, 023 (2014). https://doi.org/10.1088/1475-7516/2014/04/023. arXiv:1310.6352 [hep-ph]
22. M.W. Cahill-Rowley, J.L. Hewett, S. Hoeche, A. Ismail, T.G. Rizzo, The new look pMSSM with neutralino and gravitino LSPs. Eur. Phys. J. C **72**, 2156 (2012). https://doi.org/10.1140/epjc/s10052-012-2156-1. arXiv:1206.4321 [hep-ph]
23. F. Maltoni, A. Martini, K. Mawatari, B. Oexl, Signals of a superlight gravitino at the LHC. JHEP **04**, 021 (2015). https://doi.org/10.1007/JHEP04(2015)021. arXiv:1502.01637 [hep-ph]
24. A. Brandenburg, L. Covi, K. Hamaguchi, L. Roszkowski, F.D. Steffen, Signatures of axinos and gravitinos at colliders. Phys. Lett. B **617**, 99–111 (2005). https://doi.org/10.1016/j.physletb.2005.04.072. arXiv:hep-ph/0501287
25. K.-Y. Choi, L. Covi, J.E. Kim, L. Roszkowski, Axino cold dark matter revisited. JHEP **04**, 106 (2012). https://doi.org/10.1007/JHEP04(2012)106. arXiv:1108.2282 [hep-ph]
26. K.-Y. Choi, J.E. Kim, L. Roszkowski, Review of axino dark matter. J. Korean Phys. Soc. **63**, 1685–1695 (2013). https://doi.org/10.3938/jkps.63.1685. arXiv:1307.3330 [astro-ph.CO]
27. L. Covi, J.E. Kim, Axinos as dark matter particles. New J. Phys. **11**, 105003 (2009). https://doi.org/10.1088/1367-2630/11/10/105003. arXiv:0902.0769 [astro-ph.CO]
28. R.T. Co, F. D'Eramo, L.J. Hall, Gravitino or axino dark matter with reheat temperature as high as 10^{16} GeV. JHEP **03**, 005 (2017). https://doi.org/10.1007/JHEP03(2017)005. arXiv:1611.05028 [hep-ph]
29. C. Cheung, G. Elor, L.J. Hall, The cosmological axino problem. Phys. Rev. D **85**, 015008 (2012). https://doi.org/10.1103/PhysRevD.85.015008. arXiv:1104.0692 [hep-ph]
30. J.L. Feng et al., The forward physics facility at the high-luminosity LHC. J. Phys. G **50**(3), 030501 (2023). https://doi.org/10.1088/1361-6471/ac865e. arXiv:2203.05090 [hep-ex]
31. D. Curtin et al., Long-lived particles at the energy frontier: the MATHUSLA physics case. Rep. Prog. Phys. **82**(11), 116201 (2019). https://doi.org/10.1088/1361-6633/ab28d6. arXiv:1806.07396 [hep-ph]
32. D.J.H. Chung, L.L. Everett, G.L. Kane, S.F. King, J.D. Lykken, L.-T. Wang, The soft supersymmetry breaking Lagrangian: theory and applications. Phys. Rep. **407**, 1–203 (2005). https://doi.org/10.1016/j.physrep.2004.08.032. arXiv:hep-ph/0312378
33. **GAMBIT** Collaboration, P. Athron et al., A global fit of the MSSM with GAMBIT. Eur. Phys. J. C **77**(12), 879 (2017). https://doi.org/10.1140/epjc/s10052-017-5196-8. arXiv:1705.07917 [hep-ph]
34. J. Pradler, F.D. Steffen, Constraints on the reheating temperature in gravitino dark matter scenarios. Phys. Lett. B **648**, 224–235 (2007). https://doi.org/10.1016/j.physletb.2007.02.072. arXiv:hep-ph/0612291
35. F.D. Steffen, Gravitino dark matter and cosmological constraints. JCAP **09**, 001 (2006). https://doi.org/10.1088/1475-7516/2006/09/001. arXiv:hep-ph/0605306
36. F.D. Steffen, Dark matter candidates—axions, neutralinos, gravitinos, and axinos. Eur. Phys. J. C **59**, 557–588 (2009). https://doi.org/10.1140/epjc/s10052-008-0830-0. arXiv:0811.3347 [hep-ph]
37. A. Freitas, F.D. Steffen, N. Tajuddin, D. Wyler, Late energy injection and cosmological constraints in axino dark matter scenarios. Phys. Lett. B **682**, 193–199 (2009). https://doi.org/10.1016/j.physletb.2009.10.094. arXiv:0909.3293 [hep-ph]
38. **Planck** Collaboration, N. Aghanim et al., Planck 2018 results. VI. Cosmological parameters. Astron. Astrophys.**641**, A6 (2020). https://doi.org/10.1051/0004-6361/201833910. arXiv:1807.06209 [astro-ph.CO]. [Erratum: Astron.Astrophys. **652**, C4 (2021)]
39. M. Lucca, N. Schöneberg, D.C. Hooper, J. Lesgourgues, J. Chluba, The synergy between CMB spectral distortions and anisotropies. JCAP **02**, 026 (2020). https://doi.org/10.1088/1475-7516/2020/02/026. arXiv:1910.04619 [astro-ph.CO]
40. Y. Gu, M. Khlopov, L. Wu, J.M. Yang, B. Zhu, Light gravitino dark matter: LHC searches and the Hubble tension. Phys. Rev. D **102**(11), 115005 (2020). https://doi.org/10.1103/PhysRevD.102.115005. arXiv:2006.09906 [hep-ph]
41. G. Choi, T.T. Yanagida, Gravitino cosmology helped by a right handed (s)neutrino. Phys. Lett. B **827**, 136954 (2022). https://doi.org/10.1016/j.physletb.2022.136954. arXiv:2104.02958 [hep-ph]
42. K. Hamaguchi, K. Nakayama, Y. Tang, Gravitino/axino as decaying dark matter and cosmological tensions. Phys. Lett. B **772**, 415–419 (2017). https://doi.org/10.1016/j.physletb.2017.06.071. arXiv:1705.04521 [hep-ph]
43. J.J. Bennett, G. Buldgen, M. Drewes, Y.Y.Y. Wong, Towards a precision calculation of the effective number of neutrinos $N_{\rm eff}$ in the Standard Model I: the QED equation of state. JCAP **03**, 003 (2020). https://doi.org/10.1088/1475-7516/2020/03/003. arXiv:1911.04504 [hep-ph]. [Addendum: JCAP **03**, A01 (2021)]
44. J.J. Bennett, G. Buldgen, P.F. De Salas, M. Drewes, S. Gariazzo, S. Pastor, Y.Y.Y. Wong, Towards a precision calculation of $N_{\rm eff}$ in the Standard Model II: neutrino decoupling in the presence of flavour oscillations and finite-temperature QED. JCAP **04**, 073 (2021). https://doi.org/10.1088/1475-7516/2021/04/073. arXiv:2012.02726 [hep-ph]
45. M. Drewes, Y. Georis, M. Klasen, L.P. Wiggering, Y.Y.Y. Wong, Towards a precision calculation of $N_{\rm eff}$ in the Standard Model III: improved estimate of NLO corrections to the collision integral. arXiv:2402.18481 [hep-ph]
46. J. Froustey, C. Pitrou, M.C. Volpe, Neutrino decoupling including flavour oscillations and primordial nucleosynthesis. JCAP **12**, 015 (2020). https://doi.org/10.1088/1475-7516/2020/12/015. arXiv:2008.01074 [hep-ph]
47. L.J. Hall, K. Jedamzik, J. March-Russell, S.M. West, Freeze-in production of FIMP dark matter. JHEP **03**, 080 (2010). https://doi.org/10.1007/JHEP03(2010)080. arXiv:0911.1120 [hep-ph]
48. G. Bélanger, G. Drieu La Rochelle, B. Dumont, R.M. Godbole, S. Kraml, S. Kulkarni, LHC constraints on light neutralino dark matter in the MSSM. Phys. Lett. B **726**, 773–780 (2013). https://doi.org/10.1016/j.physletb.2013.09.059. arXiv:1308.3735 [hep-ph]
49. R.K. Barman, G. Bélanger, B. Bhattacherjee, R.M. Godbole, R. Sengupta, Is light neutralino thermal dark matter in the phenomenological minimal supersymmetric standard model ruled out? Phys. Rev. Lett. **131**(1), 011802 (2023). https://doi.org/10.1103/PhysRevLett.131.011802. arXiv:2207.06238 [hep-ph]
50. D. Albornoz Vasquez, G. Belanger, C. Boehm, A. Pukhov, J. Silk, Can neutralinos in the MSSM and NMSSM scenarios still be light? Phys. Rev. D **82**, 115027 (2010). https://doi.org/10.1103/PhysRevD.82.115027. arXiv:1009.4380 [hep-ph]
51. D. Ghosh, R. Godbole, M. Guchait, K. Mohan, D. Sengupta, Looking for an invisible Higgs signal at the LHC. Phys. Lett. B **725**, 344–351 (2013). https://doi.org/10.1016/j.physletb.2013.07.042. arXiv:1211.7015 [hep-ph]
52. R.K. Barman, G. Bélanger, B. Bhattacherjee, R. Godbole, D. Sengupta, X. Tata, Current bounds and future prospects of light neutralino dark matter in NMSSM. Phys. Rev. D **103**(1), 015029 (2021). https://doi.org/10.1103/PhysRevD.103.015029. arXiv:2006.07854 [hep-ph]
53. K.A. Mohan, D. Sengupta, T.M.P. Tait, B. Yan, C.P. Yuan, Direct detection and LHC constraints on a t-channel simplified model of Majorana dark matter at one loop. JHEP **05**, 115 (2019). https://doi.org/10.1007/JHEP05(2019)115. arXiv:1903.05650 [hep-ph]. [Erratum: JHEP **05**, 232 (2023)]
54. M. Becker, E. Copello, J. Harz, K.A. Mohan, D. Sengupta, Impact of Sommerfeld effect and bound state formation in simplified t-

channel dark matter models. JHEP **08**, 145 (2022). https://doi.org/10.1007/JHEP08(2022)145. arXiv:2203.04326 [hep-ph]
55. S. Mizuta, M. Yamaguchi, Coannihilation effects and relic abundance of Higgsino dominant LSP(s). Phys. Lett. B **298**, 120–126 (1993). https://doi.org/10.1016/0370-2693(93)91717-2. arXiv:hep-ph/9208251
56. M. Guchait, D.P. Roy, D. Sengupta, Probing a mixed neutralino dark matter model at the 7 TeV LHC. Phys. Rev. D **85**, 035024 (2012). https://doi.org/10.1103/PhysRevD.85.035024. arXiv:1109.6529 [hep-ph]
57. G. F. Giudice, A. Romanino, Split supersymmetry. Nucl. Phys. B **699**, 65–89 (2004). https://doi.org/10.1016/j.nuclphysb.2004.08.001. arXiv:hep-ph/0406088. [Erratum: Nucl. Phys. B **706**, 487–487 (2005)]
58. N. Cribiori, D. Lust, M. Scalisi, The gravitino and the swampland. JHEP **06**, 071 (2021). https://doi.org/10.1007/JHEP06(2021)071. arXiv:2104.08288 [hep-th]
59. A. Strumia, Thermal production of axino Dark Matter. JHEP **06**, 036 (2010). https://doi.org/10.1007/JHEP06(2010)036. arXiv:1003.5847 [hep-ph]
60. **Particle Data Group** Collaboration, R.L. Workman et al., Review of particle physics. PTEP**2022**, 083C01 (2022). https://doi.org/10.1093/ptep/ptac097
61. S.K. Acharya, R. Khatri, CMB anisotropy and BBN constraints on pre-recombination decay of dark matter to visible particles. JCAP **12**, 046 (2019). https://doi.org/10.1088/1475-7516/2019/12/046. arXiv:1910.06272 [astro-ph.CO]
62. M. Kawasaki, T. Moroi, Electromagnetic cascade in the early universe and its application to the big bang nucleosynthesis. Astrophys. J. **452**, 506 (1995). https://doi.org/10.1086/176324. arXiv:astro-ph/9412055
63. R.J. Protheroe, T. Stanev, V.S. Berezinsky, Electromagnetic cascades and cascade nucleosynthesis in the early universe. Phys. Rev. D **51**, 4134–4144 (1995). https://doi.org/10.1103/PhysRevD.51.4134. arXiv:astro-ph/9409004
64. J. Chluba, D. Jeong, Teasing bits of information out of the CMB energy spectrum. Mon. Not. R. Astron. Soc. **438**(3), 2065–2082 (2014). https://doi.org/10.1093/mnras/stt2327. arXiv:1306.5751 [astro-ph.CO]
65. M. Kawasaki, K. Kohri, T. Moroi, Big-Bang nucleosynthesis and hadronic decay of long-lived massive particles. Phys. Rev. D **71**, 083502 (2005). https://doi.org/10.1103/PhysRevD.71.083502. arXiv:astro-ph/0408426
66. V. Poulin, P.D. Serpico, Nonuniversal BBN bounds on electromagnetically decaying particles. Phys. Rev. D **91**(10), 103007 (2015). https://doi.org/10.1103/PhysRevD.91.103007. arXiv:1503.04852 [astro-ph.CO]
67. V. Poulin, J. Lesgourgues, P.D. Serpico, Cosmological constraints on exotic injection of electromagnetic energy. JCAP **03**, 043 (2017). https://doi.org/10.1088/1475-7516/2017/03/043. arXiv:1610.10051 [astro-ph.CO]
68. K. Griest, M. Kamionkowski, Unitarity limits on the mass and radius of dark matter particles. Phys. Rev. Lett. **64**, 615 (1990). https://doi.org/10.1103/PhysRevLett.64.615
69. H. Tashiro, CMB spectral distortions and energy release in the early universe. PTEP **2014**(6), 06B107 (2014). https://doi.org/10.1093/ptep/ptu066
70. J. Chluba, J. Hamann, S.P. Patil, Features and new physical scales in primordial observables: theory and observation. Int. J. Mod. Phys. D **24**(10), 1530023 (2015). https://doi.org/10.1142/S0218271815300232. arXiv:1505.01834 [astro-ph.CO]
71. J.C. Mather et al., A preliminary measurement of the cosmic microwave background spectrum by the cosmic background explorer (COBE) satellite. Astrophys. J. Lett. **354**, L37–L40 (1990). https://doi.org/10.1086/185717
72. D.J. Fixsen, E.S. Cheng, J.M. Gales, J.C. Mather, R.A. Shafer, E.L. Wright, The cosmic microwave background spectrum from the full COBE FIRAS data set. Astrophys. J. **473**, 576 (1996). https://doi.org/10.1086/178173. arXiv:astro-ph/9605054
73. **PRISM** Collaboration, P. André et al., PRISM (polarized radiation imaging and spectroscopy mission): an extended white paper. JCAP **02**, 006 (2014). https://doi.org/10.1088/1475-7516/2014/02/006. arXiv:1310.1554 [astro-ph.CO]
74. K. Jedamzik, M. Lemoine, G. Moultaka, Gravitino, axino, Kaluza–Klein graviton warm and mixed dark matter and reionisation. JCAP **07**, 010 (2006). https://doi.org/10.1088/1475-7516/2006/07/010. arXiv:astro-ph/0508141
75. G. Ballesteros, M.A.G. Garcia, M. Pierre, How warm are non-thermal relics? Lyman-α bounds on out-of-equilibrium dark matter. JCAP **03**, 101 (2021). https://doi.org/10.1088/1475-7516/2021/03/101. arXiv:2011.13458 [hep-ph]
76. Q. Decant, J. Heisig, D.C. Hooper, L. Lopez-Honorez, Lyman-α constraints on freeze-in and superWIMPs. JCAP **03**, 041 (2022). https://doi.org/10.1088/1475-7516/2022/03/041. arXiv:2111.09321 [astro-ph.CO]
77. V. Iršič et al., New constraints on the free-streaming of warm dark matter from intermediate and small scale Lyman-α forest data. Phys. Rev. D **96**(2), 023522 (2017). https://doi.org/10.1103/PhysRevD.96.023522. arXiv:1702.01764 [astro-ph.CO]
78. **DES** Collaboration, E.O. Nadler et al., Milky Way Satellite Census. III. Constraints on dark matter properties from observations of milky way satellite galaxies. Phys. Rev. Lett. **126**, 091101 (2021).https://doi.org/10.1103/PhysRevLett.126.091101. arXiv:2008.00022 [astro-ph.CO]
79. A. Boyarsky, J. Lesgourgues, O. Ruchayskiy, M. Viel, Lyman-alpha constraints on warm and on warm-plus-cold dark matter models. JCAP **05**, 012 (2009). https://doi.org/10.1088/1475-7516/2009/05/012. arXiv:0812.0010 [astro-ph]
80. **GAMBIT** Collaboration, V. Ananyev et al., Collider constraints on electroweakinos in the presence of a light gravitino. Eur. Phys. J. C **83**(6), 493 (2023). https://doi.org/10.1140/epjc/s10052-023-11574-z. arXiv:2303.09082 [hep-ph]
81. N. Arkani-Hamed, S. Dimopoulos, Supersymmetric unification without low energy supersymmetry and signatures for fine-tuning at the LHC. JHEP **06**, 073 (2005). https://doi.org/10.1088/1126-6708/2005/06/073. arXiv:hep-th/0405159
82. **DELPHI** Collaboration, J. Abdallah et al., Photon events with missing energy in e+ e- collisions at s**(1/2) = 130-GeV to 209-GeV. Eur. Phys. J. C **38**, 395–411 (2005). https://doi.org/10.1140/epjc/s2004-02051-8. arXiv:hep-ex/0406019
83. G.F. Giudice, R. Rattazzi, Theories with gauge mediated supersymmetry breaking. Phys. Rep. **322**, 419–499 (1999). https://doi.org/10.1016/S0370-1573(99)00042-3. arXiv:hep-ph/9801271
84. **ATLAS** Collaboration, G. Aad et al., Search for nonpointing and delayed photons in the diphoton and missing transverse momentum final state in 8 TeV pp collisions at the LHC using the ATLAS detector. Phys. Rev. D **90**(11), 112005 (2014). https://doi.org/10.1103/PhysRevD.90.112005. arXiv:1409.5542 [hep-ex]
85. **CMS** Collaboration, Search for long-lived particles using delayed photons with proton-proton collisions at $\sqrt{s} = 13$ TeV
86. **CHARM** Collaboration, F. Bergsma et al., A search for decays of heavy neutrinos. Phys. Lett. B **128**, 361 (1983). https://doi.org/10.1016/0370-2693(83)90275-7
87. S.N. Gninenko, Constraints on sub-GeV hidden sector gauge bosons from a search for heavy neutrino decays. Phys. Lett. B **713**, 244–248 (2012). https://doi.org/10.1016/j.physletb.2012.06.002. arXiv:1204.3583 [hep-ph]
88. **NA62** Collaboration, B. Döbrich, Dark sectors at fixed targets: the example of NA62. Frascati Phys. Ser. **66**, 312–327 (2018). arXiv:1807.10170 [hep-ex]

89. **NOMAD** Collaboration, P. Astier et al., Search for heavy neutrinos mixing with tau neutrinos. Phys. Lett. B **506**, 27–38 (2001). https://doi.org/10.1016/S0370-2693(01)00362-8. arXiv:hep-ex/0101041
90. **SHiP** Collaboration, M. Anelli et al., A facility to search for hidden particles (SHiP) at the CERN SPS. arXiv:1504.04956 [physics.ins-det]
91. A. Berlin, S. Gori, P. Schuster, N. Toro, Dark sectors at the fermilab seaquest experiment. Phys. Rev. D **98**, 035011 (2018). https://doi.org/10.1103/PhysRevD.98.035011
92. K.-Y. Choi, T. Inami, K. Kadota, I. Park, O. Seto, Searching for axino-like particle at fixed target experiments. Phys. Dark Univ. **27**, 100460 (2020). https://doi.org/10.1016/j.dark.2020.100460. arXiv:1902.10475 [hep-ph]
93. K. Jodłowski, Looking forward to photon-coupled long-lived particles IV: neutralino-ALPino/gravitino. arXiv:2306.00982 [hep-ph]
94. P.W. Graham, D.E. Kaplan, S. Rajendran, Cosmological relaxation of the electroweak scale. Phys. Rev. Lett. **115**(22), 221801 (2015). https://doi.org/10.1103/PhysRevLett.115.221801. arXiv:1504.07551 [hep-ph]
95. G.F. Giudice, M. McCullough, A clockwork theory. JHEP **02**, 036 (2017). https://doi.org/10.1007/JHEP02(2017)036. arXiv:1610.07962 [hep-ph]
96. A. Goudelis, K.A. Mohan, D. Sengupta, Clockworking FIMPs. JHEP **10**, 014 (2018). https://doi.org/10.1007/JHEP10(2018)014. arXiv:1807.06642 [hep-ph]
97. J.L. Feng, A. Rajaraman, F. Takayama, Graviton cosmology in universal extra dimensions. Phys. Rev. D **68**, 085018 (2003). https://doi.org/10.1103/PhysRevD.68.085018. arXiv:hep-ph/0307375
98. C. Csáki, S. Hong, G. Kurup, S.J. Lee, M. Perelstein, W. Xue, Continuum dark matter. Phys. Rev. D **105**(3), 035025 (2022). https://doi.org/10.1103/PhysRevD.105.035025. arXiv:2105.07035 [hep-ph]